Impact of different extended components of mean-field models on transport coefficients of quark matter and their causal aspects

Chowdhury Aminul Islam*
Department of Theoretical Physics, Tata Institute of Fundamental Research, Homi Bhabha Road, Mumbai 400005, India

Jayanta Dey† and Sabyasachi Ghosh‡
Indian Institute of Technology Bhilai, GEC Campus, Sejbahar, Raipur 492015, Chhattisgarh, India

(Received 6 March 2019; revised 2 January 2021; accepted 2 February 2021; published 15 March 2021)

The role of different extensions of the Nambu-Jona-Lasinio (NJL) model-like addition of vector interaction, Polyakov loop extended version (PNJL), and the entangled PNJL (EPNJL) models on transport coefficients, such as shear viscosity, bulk viscosity, electrical conductivity, and thermal conductivity are critically analyzed. We have considered the standard expressions of transport coefficients, obtained in relaxation time approximation of kinetic theory. Influence of temperature-dependent order parameters on the temperature profile of transport coefficients are analyzed. The causal aspect of the massless case to these different extended components of mean-field models are also picturized where an approximated lower and upper bound are drawn for shear relaxation time.

DOI: 10.1103/PhysRevC.103.034904

I. INTRODUCTION

Microscopic calculations of transport coefficients for highly dense quark matter, which may be seen in astrophysical objects, such as compact stars, are an important input in modeling an array of astrophysical phenomena. References [1–4] have gone through these microscopic estimations. Future experimental facilities, such as Facility for Antiproton and Ion Research at GSI, Germany [5] and the Nuclotron-based Ion Collider Facility at JINR, Russia [6] aim to probe similar kinds of high density zones in their laboratories. Transport coefficients of highly dense matter, produced there, may have influence on different phenomenological quantities, such as spectra, flow, which can be constructed from experimental data, measured by their detector setup.

On the other hand, a baryon-free hot system can also be a matter of interest to know its transport coefficients values. It is believed that our early universe went through this state, just after few microseconds from the big bang. Relativistic Heavy Ion Collider (RHIC) experiments at Brookhaven National Laboratory, USA and the Large Hadron Collider (LHC) experiments at CERN, Switzerland had reached this high temperature and baryon free zone, and their experimental data [7–12] indicate that the matter almost behave, such as a nearly perfect fluid. A very small value of shear viscosity to entropy density ratio η/s corresponds to this nature, and this small value of η/s has been searched as input guess values in the viscous hydrodynamic model analysis during the matching experimental data of elliptic flow [13–15]. This small value of η/s from the experimental side throws a challenge to the theoretical side where microscopic calculations of η/s for quark matter can be performed. Estimated values of η/s from perturbative quantum chromodynamics at leading order [16,17] are found to be quite larger than their experimental value. However, Ref. [18] has recently found a significant drop in this value in the next-to-leading order calculation, but at the end of the article, the possibility of nonperturbative components in η/s has not been ruled out. The nonperturbative temperature domain of QCD can be well mimicked by effective QCD model calculations, such as the Nambu-Jona-Lasinio (NJL) model and quark-meson models. In Refs. [19–31], this type microscopic calculation of shear viscosity via different effective QCD models has been performed. Among them, Refs. [19–28] have adopted the NJL model, Ref. [31] has further incorporated the background gauge field through its Polyakov extended version. There are many possible additional sources by which the NJL model can be modified into different versions. For example, addition of the vector interaction and Polyakov loop extension, entangled Polyakov loop extensions can modify the NJL model structure. In the present article, we have tried to investigate the impact of the different additional sources of the NJL model on η/s calculations as well as for other transport coefficients, such as bulk viscosity, electrical conductivity, and thermal conductivity.

The article is organized as follows. In Sec. II, the formalism part of different versions of the NJL model has been briefly addressed and in Sec. III, the expressions of different transport coefficients are derived in the kinetic theory framework along

*chowdhury.aminulislam@gmail.com
†jayantad@iitbhilai.ac.in
‡sabyaphy@gmail.com

with their causal extensions. Then, Sec. IV has provided the detail numerical discussion, which has explored the impact of different extensions of the NJL model on the transport coefficient and at last, we have summarized our studies.

II. FORMALISM OF THE NJL MODEL WITH DIFFERENT EXTENSIONS

In this section we briefly discuss the mean-field models that we have employed in our paper. First we talk about the NJL model for two flavor cases and introduce vector interaction in the picture. Then we extend it by introducing the Polyakov loop field known as the PNJL model, through which the deconfinement dynamics can be mimicked. In the PNJL model the correlation between the chiral and the deconfinement dynamics is weak. We impose a strong correlation between these two through Polyakov loop-dependent coupling constants—this is known as the entangled PNJL (EPNJL) model.

A. NJL

Let us start with the NJL model first. Here we are interested in two light quark flavors, and we include the isoscalar vector interaction which plays a crucial role specially for the system with finite density. The Lagrangian is [32–35] as follows:

$$\mathcal{L}_{\rm NJL} = \bar{\psi}(i\gamma_\mu\partial^\mu - m_0 + \gamma_0\mu)\psi + \frac{G_S}{2}[(\bar{\psi}\psi)^2 + (\bar{\psi}i\gamma_5\vec{\tau}\psi)^2] - \frac{G_V}{2}(\bar{\psi}\gamma_\mu\psi)^2, \quad (1)$$

where, $m_0 = m_0 \times \mathbf{1}$, with $\mathbf{1}$ being the identity matrix and $m_u = m_d = m_0$; μ is the chemical potential; $\vec{\tau}$ is the Pauli matrix; G_S and G_V are the four-scalar- and isoscalar-vector-type coupling constants, respectively. The value of G_V is not fixed through parameter fitting, rather it is used as a free parameter which can take values within the range of $0 \leqslant G_V/G_S \leqslant 1$. With the inclusion of the vector interaction, we now have another condensate as quark number density $n = \langle\bar{\psi}\gamma^0\psi\rangle$ [35,36] along with the usual chiral condensate $\Sigma = \langle\bar{\psi}\psi\rangle$. Chiral condensate will build the link between current quark mass m_0 and constituent quark mass M via the relation,

$$M = m_0 + 2G_S N_c N_f \int \frac{d^3\boldsymbol{p}}{(2\pi)^3}\frac{M}{E}(1 - f_Q - f_{\bar{Q}}), \quad (2)$$

where

$$f_{Q,\bar{Q}} = \frac{1}{e^{(E\mp\tilde{\mu})/T} + 1}, \quad (3)$$

and quark number density make the quark chemical potential μ shift to an effective chemical potential,

$$\tilde{\mu} = \mu - G_V n. \quad (4)$$

Since, NJL is not renormalizable, we regularize the diverging vacuum integral by introducing a sharp three-momentum cutoff Λ. The energy of the quasiquark (both up and down) of constituent mass M is given as $E = \sqrt{\boldsymbol{p}^2 + M^2}$. The chiral condensate Σ at finite temperature depends on the Fermi-Dirac (FD) distribution function, which is the function of the effective chemical potential, given in Eq. (4). Hence, G_V dependence enters in the gap equation through this thermodynamical phase space. This gap Eq. (2) is plotted in Fig. 1 for different values of G_V, and we find a mild noticeable enhancement of M with G_V in the intermediate temperature range. Decreasing in the quark chemical potential with G_V make thermal parts shrink. Therefore, the contribution of the [vacuum-thermal] term on the left-hand side of (self-consistent) Eq. (2) is increased for which we are getting an increasing trend of M with G_V. We can get back to the usual NJL Lagrangian by switching the vector interaction off.

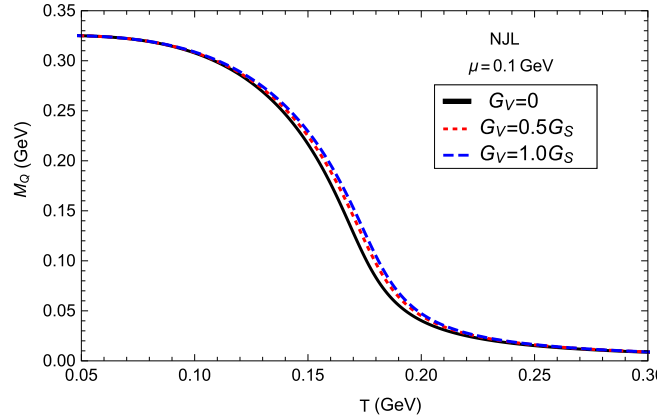

FIG. 1. Temperature dependence of constituent quark masses for $\frac{G_V}{G_S} = 0$ (solid line), 0.5 (dotted line), 1 (dashed line) at $\mu =$ 0.1 GeV.

With all these in hand, we can now write the thermodynamic potential using the mean-field approximation as

$$\Omega_{\rm NJL} = \frac{G_S}{2}\Sigma^2 - \frac{G_V}{2}n^2 - 2N_f N_c\int_\Lambda \frac{d^3\boldsymbol{p}}{(2\pi)^3}E - 2N_f N_c T\int\frac{d^3\boldsymbol{p}}{(2\pi)^3}[\ln(1 + e^{-(E-\tilde{\mu})/T}) + \ln(1 + e^{-(E+\tilde{\mu})/T})]. \quad (5)$$

The thermodynamic potential depends on both constituent quark mass (M) and the effective chemical potential ($\tilde{\mu}$).

B. PNJL

So far we have considered only the chiral dynamics by which quark to hadron phase transition can be realized as restored to broken phases of chiral symmetry. Now we also incorporate the deconfinement dynamics by including the Polyakov loop. It will give us another view where we can see the quark to hadron phase transition as a confinement to deconfinement phase transition. This is formally known as the PNJL model [37–42]. Here along with the Σ and n fields we have two more mean fields—expectation value of Polyakov loop Φ and its conjugate $\bar{\Phi}$. Φ works as the order parameter for deconfinement dynamics. For two flavors the PNJL Lagrangian with vector interaction is written as

$$\mathcal{L}_{\rm PNJL} = \bar{\psi}(i\not{D} - m_0 + \gamma_0\mu)\psi + \frac{G_S}{2}[(\bar{\psi}\psi)^2 + (\bar{\psi}i\gamma_5\vec{\tau}\psi)^2] - \frac{G_V}{2}(\bar{\psi}\gamma_\mu\psi)^2 - \mathcal{U}(\Phi[A], \bar{\Phi}[A], T), \quad (6)$$

where $\not{D} = \gamma_\mu D^\mu$ and the covariant derivative $D^\mu = \partial^\mu - ig\mathcal{A}^\mu_a \lambda_a/2$, $\mathcal{A}^\mu_a = \delta^{\mu 0}\mathcal{A}^a_0$ being the SU(3) background fields; λ_a's are the Gell-Mann matrices. One should note that here only two components of the gauge field, corresponding to λ_3 and λ_8, will contribute. The effective Polyakov loop gauge potential is parameterized as

$$\frac{\mathcal{U}(\Phi, \bar{\Phi}, T)}{T^4} = -\frac{b_2(T)}{2}\Phi\bar{\Phi} - \frac{b_3}{6}(\Phi^3 + \bar{\Phi}^3) + \frac{b_4}{4}(\bar{\Phi}\Phi)^2, \tag{7}$$

with

$$b_2(T) = a_0 + a_1\left(\frac{T_0}{T}\right) + a_2\left(\frac{T_0}{T}\right)^2 + a_3\left(\frac{T_0}{T}\right)^3. \tag{8}$$

Values of different coefficients and parameters a_0, a_1, a_2, a_3, b_3, b_4, T_0, and κ are the same as those given in Refs. [40,43]. We should note an important point here that in the NJL model the color trace gives us a factor of N_c. In the presence of a background gauge field the color trace is not straightforward. After some mathematical manipulation the color trace in the PNJL model also splits out a factor of N_c along with a modified thermal distribution function for particle and antiparticle which read as [43,44]

$$f_Q = \frac{\Phi e^{-\beta(E-\tilde{\mu})} + 2\bar{\Phi}e^{-2\beta(E-\tilde{\mu})} + e^{-3\beta(E-\tilde{\mu})}}{1 + 3\Phi e^{-\beta(E-\tilde{\mu})} + 3\bar{\Phi}e^{-2\beta(E-\tilde{\mu})} + e^{-3\beta(E-\tilde{\mu})}},$$
$$f_{\bar{Q}} = \frac{\bar{\Phi} e^{-\beta(E+\tilde{\mu})} + 2\Phi e^{-2\beta(E+\tilde{\mu})} + e^{-3\beta(E+\tilde{\mu})}}{1 + 3\bar{\Phi}e^{-\beta(E+\tilde{\mu})} + 3\Phi e^{-2\beta(E+\tilde{\mu})} + e^{-3\beta(E+\tilde{\mu})}}, \tag{9}$$

respectively. We get back the usual NJL results from these distribution functions by putting $\Phi = \bar{\Phi} = 1$. Thus, while calculating different transport coefficients in the ambient of these models one needs to be careful. For the NJL model it will be sufficient to replace the usual mass by the effective one. But for the PNJL model one also needs to incorporate the modified distribution functions (see Ref. [30]). With these modified distribution functions the effective mass in the PNJL model reads as

$$M = m_0 + 2G_S N_c N_f \int \frac{d^3\boldsymbol{p}}{(2\pi)^3}\frac{M}{E}(1 - f_Q - f_{\bar{Q}}). \tag{10}$$

The corresponding thermodynamic potential is written as

$$\Omega_{\rm PNJL} = \mathcal{U}(\Phi, \bar{\Phi}, T) + \frac{G_S}{2}\Sigma^2 - \frac{G_V}{2}n^2 - 2N_f T\int \frac{d^3\boldsymbol{p}}{(2\pi)^3}\ln[1 + 3(\Phi + \bar{\Phi}e^{-(E-\tilde{\mu})/T})e^{-(E-\tilde{\mu})/T} + e^{-3(E-\tilde{\mu})/T}]$$
$$-2N_f T\int \frac{d^3\boldsymbol{p}}{(2\pi)^3}\ln[1 + 3(\bar{\Phi} + \Phi e^{-(E+\tilde{\mu})/T})e^{-(E+\tilde{\mu})/T} + e^{-3(E+\tilde{\mu})/T}] - \kappa T^4 \ln[J(\Phi, \bar{\Phi})] - 2N_f N_c\int_\Lambda \frac{d^3\boldsymbol{p}}{(2\pi)^3}E. \tag{11}$$

The Vandermonde determinant $J(\Phi, \bar{\Phi})$ is given by [40,45]

$$J[\Phi, \bar{\Phi}] = \frac{27}{24\pi^2}[1 - 6\Phi\bar{\Phi} + 4(\Phi^3 + \bar{\Phi}^3) - 3(\Phi\bar{\Phi})^2]. \tag{12}$$

C. EPNJL

It has been confirmed through a different lattice QCD (LQCD) simulation that chiral and deconfinement transitions take place at the same temperature [46] or nearly the same temperature [47]. Now this is not clearly understood whether it is a mere coincidence or there are some correlations between these two apparently distinct phenomena. To understand this coincidence through effective models a conjecture of strong entanglement between the chiral and the deconfinement dynamics has been proposed [48,49]. Because of this entanglement of two dynamics it is known as the EPNJL model. This is realized by introducing Polyakov loop-dependent coupling constants where the form of the ansatz is so chosen that it is Z_3 symmetric. Thus, the Lagrangian in the EPNJL model is the same as that in Eq. (6) except the coupling constants G_S and G_V are now replaced by $\tilde{G}_S(\Phi)$ and $\tilde{G}_V(\Phi)$. They are given by

$$\tilde{G}_S(\Phi) = G_S[1 - \alpha_1\Phi\bar{\Phi} - \alpha_2(\Phi^3 + \bar{\Phi}^3)], \tag{13}$$

and

$$\tilde{G}_V(\Phi) = G_V[1 - \alpha_1\Phi\bar{\Phi} - \alpha_2(\Phi^3 + \bar{\Phi}^3)]. \tag{14}$$

If we put $\alpha_1 = \alpha_2 = 0$ we get back the usual PNJL model. The strength of the vector coupling constant is as mentioned earlier taken in terms of values of G_S. In the same way we can get the thermodynamic potential for the EPNJL model by introducing Polyakov loop-dependent coupling constants in Eq. (11). Now along with all the parameters in the PNJL model we have two new parameters α_1 and α_2 which need to be fixed. This is performed and discussed in detail in Ref. [50]. It is found there that the values of $(\alpha_1, \alpha_2) = (0.1, 0.1)$ allow to reproduce the coincidence of two transition temperatures to be within the range provided by the lattice QCD for the zero chemical potential [51,52]. The explicit form of the gap equation in the EPNJL model is the same as that written in Eq. (10) except that G_S and G_V will now be replaced by $\tilde{G}_S$ and $\tilde{G}_V$ as given in Eqs. (13) and (14), respectively.

The picture of transition from a current quark mass $m_0 \approx 0.010$ GeV at high T to constituent quark mass $M \approx 0.320$ GeV at low T will mainly map the quark-hadron phase transition, and the maximum transition of mass is occurring at the transition temperature point. In different extended NJL models, this point is shifted. Figure 2 demonstrates it nicely.

Let us start with the discussion of transition temperature for the NJL model first. From the melting of the $M(T)$ curve (red solid line) for the NJL model, one can recognize roughly the maximum melting point as $T_\Sigma \approx 0.177$ GeV (at $\mu = 0$). It is only chiral dynamics which is associated with this mass melting in the NJL model, therefore, T_Σ is popularly known as the chiral transition temperature. As we increase μ the transition temperature keeps on decreasing. On the other hand, in the PNJL model we have both chiral and deconfinement dynamics. So essentially, we have two phase transitions—one is the chiral phase transition, occurring at T_Σ, and the other

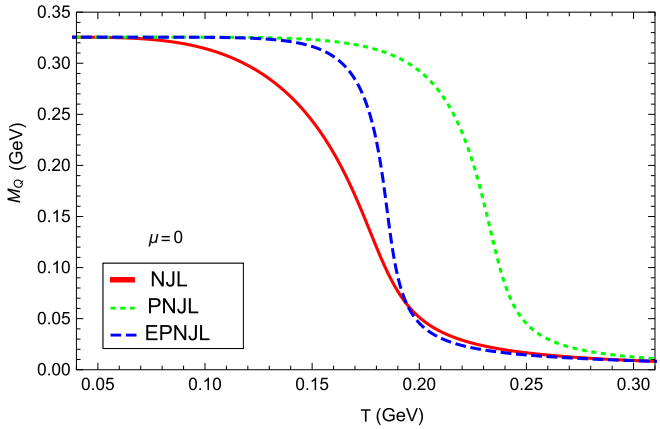

FIG. 2. Temperature dependence of constituent quark masses for NJL (solid line), PNJL (dotted line), and EPNJL (dashed line) at $\mu = 0$.

is the deconfinement phase transition, occurring at temperature T_Φ (say). In the PNJL model at $\mu = 0$, we have found $T_\Sigma = 0.233$ and $T_\Phi = 0.228$ GeV (for $\mu = 0$, $\Phi = \bar{\Phi}$, so we have $T_\Phi = T_{\bar{\Phi}}$) by searching the inflection points of the quark condensate and Polyakov loop, respectively.[1] As we increase μ both transition temperatures decrease, and there is now differences between T_Φ and $T_{\bar{\Phi}}$ for nonzero μ although very small. We take the average of the two temperatures $(\frac{T_\Phi + T_{\bar{\Phi}}}{2})$ to denote the deconfinement temperatures for nonzero values of μ. Since the chiral transition temperature is always very close to the deconfinement transition temperature, we use the average of the two $(\frac{T_\Sigma + T_\Phi}{2})$ to denote as the critical temperature in the PNJL model. In the EPNJL model with the parameter choice $(\alpha_1,\ \alpha_2) = (0.1, 0.1)$ we get $T_\Sigma = 185$ and $T_\Phi = 183$ MeV at $\mu = 0$ [50].

D. Thermodynamical quantities

We see that the thermal distributions, denoted by $f_{Q,\bar{Q}}$, are taking different forms in different versions of the model. In the NJL model it is the usual FD distribution function with effective mass (M_Q) and chemical potential ($\tilde{\mu}$) as given in Eq. (3). In the absence of vector interaction, $\tilde{\mu}$ reduces to μ. When we deal with the PNJL model the FD distributions transform to some modified forms as given in Eq. (9). Apart from these palpable differences in forms, distributions in the NJL and PNJL models are also different through the constituent quark masses, which are different for these two models (see Fig. 2). The form of the distributions remain the same in the PNJL and EPNJL models, but quantitatively they are again different because of their differences in effective mass (Fig. 2).

Now, in general, if we denote $f_{Q\bar{Q}}$ as thermal distribution functions, then we can present our different thermodynamical quantities in terms of $f_{Q\bar{Q}}$, owing to the quasiparticle relation of statistical mechanics. Thermodynamical quantities, such as pressure P, energy density ϵ, and net quark or baryon density ρ can be obtained from the quasiparticle relations [27],

$$P = 2N_f N_c \int \frac{d^3\boldsymbol{p}}{(2\pi)^3} \frac{\boldsymbol{p}^2}{3E} [f_Q + f_{\bar{Q}}], \tag{15}$$

$$\epsilon = 2N_f N_c \int \frac{d^3\boldsymbol{p}}{(2\pi)^3} E [f_Q + f_{\bar{Q}}], \tag{16}$$

$$\rho = 2N_f N_c \int \frac{d^3\boldsymbol{p}}{(2\pi)^3} [f_Q - f_{\bar{Q}}]. \tag{17}$$

The entropy density s and the heat function h are related to the above quantities through the following relations:

$$s = \frac{\epsilon + P - \mu\rho}{T}, \tag{18}$$

$$h = (\epsilon + P)/\rho. \tag{19}$$

Heat function h is an important quantity, defined by the ratio of enthalpy density $(\epsilon + P)$ to the net quark density (ρ). This quantity becomes divergent (unphysical) at $\mu = 0$ where net quark density vanishes. However, enthalpy density $h\rho = \epsilon + P$ remains finite.

III. TRANSPORT COEFFICIENTS

A detail derivation of the expressions of transport coefficients from relaxation time approximation (RTA) can be seen in Refs. [28,53–57] and from the Kubo approach in Refs. [58–60]. In this section, we will take a revisit of RTA methodology just for a sequential description.

To calculate different transport coefficients of relativistic fluid, the necessary macroscopic quantities are the energy-momentum tensor ($T^{\mu\nu}$), the four-dimensional quark-baryon current (N^μ), and the electric current (J^μ). Here, four-vectors are represented by greek letters, and three-vectors are represented by latin letters. If we consider that the fluid is made up of a two-flavor quark and antiquark, then in microscopic kinetic theory the macroscopic quantities can be expressed as

$$T^{\mu\nu} = 2N_f N_c \int \frac{d^3\boldsymbol{p}}{(2\pi)^3} \frac{p^\mu p^\nu}{E} (f_Q + f_{\bar{Q}}), \tag{20}$$

$$N^\mu = 2N_f N_c \int \frac{d^3\boldsymbol{p}}{(2\pi)^3} \frac{p^\mu}{E} (f_Q - f_{\bar{Q}}), \tag{21}$$

and

$$J^\mu = 2N_c \sum_{u,d} \int \frac{d^3\boldsymbol{p}}{(2\pi)^3} \frac{p^\mu}{E} (e_Q f_Q + e_{\bar{Q}} f_{\bar{Q}}), \tag{22}$$

where flavor degeneracy $N_f = 2$; color degeneracy $N_c = 3$; the summation stands for the two-flavor quark and antiquark to account for their charges ($e_{u,\bar{u}} = \pm 2e/3$ and $e_{d,\bar{d}} = \mp e/3$); particle four-momentum $p^\mu = (E, \boldsymbol{p})$; $E = \sqrt{\boldsymbol{p}^2 + m^2}$ for particle mass $p^\mu = (E, \boldsymbol{p})$; $E =$

[1]These inflection points can be found by plotting the first temperature derivative of Σ or Φ as a function of temperature and finding the maximum of the corresponding plot, which signifies the transition temperature T_Σ or T_Φ, respectively. In other words, these are the points at which the curvature changes sign. The readers might look into Refs. [39,40,50] for a detailed discussion, particularly, Ref. [50] which involves the same parameter set as used in the present calculation.

$\sqrt{\boldsymbol{p}^2+m^2}$ are nonequilibrium distribution functions of quarks and antiquarks, respectively. Splitting $f_{Q,\bar{Q}}$ by the equilibrium (Fermi-Dirac or modified) distribution $f^0_{Q,\bar{Q}}$ and a small deviation $\delta f_{Q,\bar{Q}}$ for the quark and antiquark, i.e.,

$$f_{Q,\bar{Q}} = f^0_{Q,\bar{Q}} + \delta f_{Q,\bar{Q}}, \tag{23}$$

one can separate out the ideal and dissipation parts of $T^{\mu\nu}$, N^μ, and J^μ as

$$T^{\mu\nu} = T^{\mu\nu}_0 + T^{\mu\nu}_D, \tag{24}$$

$$N^\mu = N^\mu_0 + N^\mu_D, \tag{25}$$

and

$$J^\mu = J^\mu_0 + J^\mu_D. \tag{26}$$

Here, the reversible-ideal part of the energy momentum tensor is $T^{\mu\nu}_0 = -g^{\mu\nu}P + (\epsilon + P)u^\mu u^\nu$, and N^μ_0, J^μ_0 are that of the quark-baryon charge current and electric charge current, respectively. The dissipation parts of two currents are N^μ_D, J^μ_D and for the energy-momentum tensor are as follows:

$$T^{\mu\nu}_D = W^\mu u^\nu + W^\nu u^\mu + \pi^{\mu\nu} + \Pi^{\mu\nu}, \tag{27}$$

where W^μ represents the energy flow, $\pi^{\mu\nu}$ and $\Pi^{\mu\nu}$ are shear and bulk viscous stress tensors, respectively. All the dissipative candidates $\pi^{\mu\nu}$, $\Pi^{\mu\nu}$, W^μ, and N^μ_D are orthogonal to the four-velocity of fluid element u^μ. They can be extracted from $T^{\mu\nu}$ and N^μ by their respective connections [61],

$$\begin{aligned} \pi^{\mu\nu} &= \left\{\tfrac{1}{2}\left(\Delta^\mu_\sigma\Delta^\nu_\rho + \Delta^\mu_\rho\Delta^\nu_\sigma\right) - \tfrac{1}{3}\Delta^{\mu\nu}\Delta_{\sigma\rho}\right\}T^{\sigma\rho}, \\ \Pi + P &= -\tfrac{1}{3}\Delta_{\mu\nu}T^{\mu\nu}, \\ q^\mu &= W^\mu - hN^\mu_D = u_\nu T^{\nu\sigma}\Delta^\mu_\sigma - h\,\Delta^\mu_\nu N^\nu. \end{aligned} \tag{28}$$

Here, the projection operator orthogonal to fluid velocity is $\Delta^{\mu\nu} = g^{\mu\nu} - u^\mu u^\nu$, Π, and P are, respectively, bulk and local isotropic pressure. In practice, four-velocity u^μ is chosen in two ways, known as Eckart and Landau frames. In the Eckart frame u^μ is parallel to N^μ and so, $N^\mu_D = 0$. Similarly, $W^\mu = 0$ in the Landau frame. For a system with no net charge, the four-velocity in the Eckart formalism is not well defined. Hence, in general, under this situation one should use the Landau frame.

The transport coefficients η, ζ, κ, and σ are basically proportionality constants, which make a connection between thermodynamical forces ($\pi^{\mu\nu}$, $\Pi^{\mu\nu}$, q^μ, E^μ) and the corresponding currents ($\mathcal{U}^{\mu\nu}_\eta, \mathcal{U}^{\mu\nu}_\zeta, \mathcal{U}^\mu_\kappa, J^\mu_D$) as [28,53–57,60,62]

$$\pi^{\mu\nu} = \eta\mathcal{U}^{\mu\nu}_\eta, \quad \text{with } \mathcal{U}^{\mu\nu}_\eta = \left(D^\mu u^\nu + D^\nu u^\mu - \frac{2}{3}\Delta^{\mu\nu}\partial_\rho u^\rho\right), \tag{29}$$

$$\Pi^{\mu\nu} = \Pi\Delta^{\mu\nu} = \zeta\mathcal{U}^{\mu\nu}_\zeta, \quad \text{with } \mathcal{U}^{\mu\nu}_\zeta = \Delta^{\mu\nu}\partial_\rho u^\rho \quad \text{and}$$
$$\Pi = \zeta\,\partial_\rho u^\rho, \tag{30}$$

$$q^\mu = \kappa\mathcal{U}^\mu_\kappa, \quad \text{with } \mathcal{U}^\mu_\kappa = T\Delta^{\mu\nu}\left(\frac{D_\nu T}{T} - \frac{D_\nu P}{hn}\right), \tag{31}$$

$$J^\mu_D = \sigma^{\mu\nu}E_\nu, \quad \text{with } E^\nu = (0, E^i). \tag{32}$$

Here, $D^\mu = \partial^\mu - u^\mu u^\sigma\partial_\sigma$ and $E^\mu \equiv F^{0\mu}$ contain the electric-field part only of electromagnetic field tensor $F^{\mu\nu}$. Using the Gibbs-Duhem relation,

$$\frac{D_\nu P}{\rho} = h\frac{D_\nu T}{T} - TD_\nu\left(\frac{\mu}{T}\right), \tag{33}$$

Eq. (31) can be further simplified as

$$\mathcal{U}^\mu_\kappa = \frac{T^2}{h}\Delta^{\mu\nu}D_\nu\left(\frac{\mu}{T}\right). \tag{34}$$

Now, owing to the microscopic relations, given in Eqs. (20)–(22), and then using Eq. (29), we can get

$$\pi^{\mu\nu} = 2N_fN_c\left[\frac{1}{2}\left(\Delta^\mu_\sigma\Delta^\nu_\rho + \Delta^\mu_\rho\Delta^\nu_\sigma\right) - \frac{1}{3}\Delta^{\mu\nu}\Delta_{\sigma\rho}\right] \times \int\frac{d^3\boldsymbol{p}}{(2\pi)^3}\frac{p^\sigma p^\rho}{E}(\delta f_Q + \delta f_{\bar{Q}}), \tag{35}$$

$$\Pi = 2N_fN_c\left[-\frac{1}{3}\Delta_{\mu\nu}\right]\int\frac{d^3\boldsymbol{p}}{(2\pi)^3}\frac{p^\mu p^\nu}{E}(\delta f_Q + \delta f_{\bar{Q}}), \tag{36}$$

$$q^\mu = 2N_fN_c\int\frac{d^3\boldsymbol{p}}{(2\pi)^3}\Delta^\mu_\sigma\left[\left\{u_\nu\frac{p^\nu p^\sigma}{E} - h\frac{p^\sigma}{E}\right\}\delta f_Q + \left\{u_\nu\frac{p^\nu p^\sigma}{E} + h\frac{p^\sigma}{E}\right\}\delta f_{\bar{Q}}\right], \tag{37}$$

and

$$J^\mu_D = 2N_c\sum_{Q=u,d}\int\frac{d^3\boldsymbol{p}}{(2\pi)^3}\frac{p^\mu}{E}(e_Q\delta f_Q + e_{\bar{Q}}\delta f_{\bar{Q}}). \tag{38}$$

In the local rest frame, four-velocity $u = (1, \boldsymbol{0})$, $p\cdot u = E$, and, hence, Eq. (37) can be written as

$$q^\mu = 2N_fN_c\int\frac{d^3\boldsymbol{p}}{(2\pi)^3}\frac{p^\mu}{E} \times\{(E-h)\delta f_Q + (E+h)\delta f_{\bar{Q}}\}. \tag{39}$$

The small deviation of the (Fermi-Dirac or modified) distribution function can be assumed as

$$\begin{aligned} \delta f_{Q,\bar{Q}} &= \left(f_{Q,\bar{Q}} - f^0_{Q,\bar{Q}}\right) \propto -\frac{\partial f^0_{Q,\bar{Q}}}{\partial E} \propto \beta f^0_{Q,\bar{Q}}\left(1 - f^0_{Q,\bar{Q}}\right) \\ &= \phi^{(Q,\bar{Q})}\beta f^0_{Q,\bar{Q}}\left(1 - f^0_{Q,\bar{Q}}\right), \end{aligned} \tag{40}$$

where $\phi^{(Q,\bar{Q})}$ will contribute to the dissipative part of energy-momentum tensor $T^{\mu\nu}_D$, quark-baryon charge current N^μ_D, and electric charge current J^μ_D as defined in Eqs (23)–(26). To satisfy the Landau-Lifshitz condition $u^\mu T^{\mu\nu}_D = 0$, a natural choice is to use the same tensorial decomposition as defined in Eqs. (29)–(32). Hence, $\phi^{(Q,\bar{Q})}$ can be expressed as a function of space-time and momentum as [28,53,55–57,62]

$$\phi^{(Q,\bar{Q})} = A^{(Q,\bar{Q})}_{\mu\nu}\mathcal{U}^{\mu\nu}_\eta + B^{(Q,\bar{Q})}_\mu\mathcal{U}^\mu_\kappa + C^{(Q,\bar{Q})}_\mu E^\mu + Z^{(Q,\bar{Q})}(\partial_\rho u^\rho). \tag{41}$$

The coefficient factors $A_{\mu\nu}$, B_μ, C_μ, and Z for different thermodynamical tensors $\mathcal{U}^{\mu\nu}_\eta$, $\mathcal{U}^\mu_\kappa$, E^μ, and $(\partial_\rho u^\rho)$ are associated with corresponding transport coefficients η, κ, σ, and ζ, respectively. These coefficient factors can be obtained with

the help of the Boltzmann equation,

$$\frac{\partial f_{Q,\bar{Q}}}{\partial t}+\frac{\partial x^i}{\partial t}\frac{\partial f_{Q,\bar{Q}}}{\partial x^i}+\frac{\partial p^i}{\partial t}\frac{\partial f_{Q,\bar{Q}}}{\partial p^i} =\left(\frac{\partial f_{Q,\bar{Q}}}{\partial t}\right)_{\rm col}\Rightarrow\frac{\partial f_{Q,\bar{Q}}}{\partial t}+v^i\frac{\partial f_{Q,\bar{Q}}}{\partial x^i}+F^i\frac{\partial f_{Q,\bar{Q}}}{\partial p^i} =\left(\frac{\partial f_{Q,\bar{Q}}}{\partial t}\right)_{\rm col}, \tag{42}$$

where v^i is the particle velocity and F^i is the applied force on the particle. The right-hand side of Eq. (42), representing the collisional term (accounting for the forces acting between particles in collisions), can be approximated by the Anderson-Witting collision term [63],

$$\left(\frac{\partial f_{Q,\bar{Q}}}{\partial t}\right)_{\rm col}=-\left(\frac{p^\mu u_\mu}{E}\right)\frac{\delta f_{Q,\bar{Q}}}{\tau_{Q,\bar{Q}}}. \tag{43}$$

This is the standard RTA technique, where $\tau_{Q,\bar{Q}}$ is the rough timescale required for the particle and antiparticle to relax from its nonequilibrium distribution $f_{Q,\bar{Q}}$ to the equilibrium distribution $f^0_{Q,\bar{Q}}$. Using Eq. (43) in Eq. (42) and then express that the RTA-based Boltzmann transport equation in covariant form as

$$\frac{1}{E}p^\mu\partial_\mu f_{Q,\bar{Q}}+e_{Q,\bar{Q}}F^{\mu\nu}\frac{p_\nu}{E}\frac{\partial f_{Q,\bar{Q}}}{\partial p^\mu}=-\left(\frac{p^\mu u_\mu}{E}\right)\frac{\delta f_{Q,\bar{Q}}}{\tau_{Q,\bar{Q}}}. \tag{44}$$

On the right-hand side, $\delta f_{Q,\bar{Q}}$ can be expressed in terms of corresponding tensors [$\mathcal{U}^{\mu\nu}_\eta$, $(\partial_\rho u^\rho)$, $\mathcal{U}^\mu_\kappa$, and $E^\mu\equiv F^{0\mu}$], associated with the transport coefficients (η, ζ, κ, and σ) by using Eq. (41). On the left-hand side, we will assume $f_{Q,\bar{Q}}\approx f^0_{Q,\bar{Q}}$. Let us proceed for the FD distribution of the NJL model, but the same steps can be performed for the modified distribution of the PNJL and EPNJL models if we follow the Appendix, given in Sec. VI B. We can write the FD distribution in covariant form

$$f^0_{Q,\bar{Q}}=1\Big/\left\{\exp\left(\frac{p^\mu u_\mu\mp\mu}{T}\right)+1\right\}, \tag{45}$$

where p^μ is the particle quantity (four-momentum) and u^μ, T, and μ are fluid quantities, which depend on space and time. So Eq. (44) will get the modified form,

$$\frac{1}{E}p^\mu\partial_\mu f^0_{Q,\bar{Q}}+e_{Q,\bar{Q}}F^{\mu\nu}\frac{p_\nu}{E}\frac{\partial f^0_{Q,\bar{Q}}}{\partial p^\mu} =-\left(\frac{p^\mu u_\mu}{ET}\right)\frac{1}{\tau_{Q,\bar{Q}}}\Big[A^{(Q,\bar{Q})}_{\mu\nu}\mathcal{U}^{\mu\nu}_\eta+B^{(Q,\bar{Q})}_\mu\mathcal{U}^\mu_\kappa +C^{(Q,\bar{Q})}_\mu E^\mu+Z^{(Q,\bar{Q})}(\partial_\rho u^\rho)\Big]f^0_{Q,\bar{Q}}\big(1-f^0_{Q,\bar{Q}}\big). \tag{46}$$

Now, the idea is to express the left-hand side of Eq. (46) in terms of the tensors, sitting on the right-hand side so that we can equate their coefficients on both sides and get the expressions of $A^{\mu\nu}$, B^μ, C^μ, and Z. The first term on the left-hand side in Eq. (46) can be expressed in terms of $\mathcal{U}^{\mu\nu}_\eta$, $\mathcal{U}^\mu_\kappa$, and $\partial_\rho u^\rho$ [28,53,55], whereas the second term on the left-hand side in Eq. (46) can be expressed in terms of $E^\mu\equiv F^{0\mu}$ [56,57,62], and then one can find

$$\begin{aligned}A^{(Q,\bar{Q})}_{\mu\nu}&=\tau_{Q,\bar{Q}}\frac{p_\mu p_\nu}{E},\\ B^{(Q,\bar{Q})}_\mu&=\tau_{Q,\bar{Q}}\frac{\beta p_\mu}{E}(E\mp h),\\ C^{(Q,\bar{Q})}_\mu&=\tau_{Q,\bar{Q}}\frac{e_{Q,\bar{Q}}p_\mu}{E}\end{aligned} \tag{47}$$

and

$$Z^{(Q,\bar{Q})}=\tau_{Q,\bar{Q}}\frac{1}{3E}\left[\boldsymbol{p}^2-3c_s^2\left(E^2-T^2\frac{dM^2_Q}{dT^2}\right)\right],$$

where bulk viscosity component $Z^{(Q,\bar{Q})}$ is obtained for $\mu=0$, but components of shear viscosity ($A^{(Q,\bar{Q})}_{\mu\nu}$) and electrical conductivity ($C^{(Q,\bar{Q})}_\mu$) can be used for both $\mu=0$ and $\mu\neq0$ (just by changing the distribution function). The component of thermal conductivity $B^{(Q,\bar{Q})}_\mu$ is relevant for $\mu\neq0$ as it carries the quantity-enthpy per particle h, which is diverged at $\mu=0$. The detailed calculation of the above outcome is given in Appendix 1.

Now, using Eqs. (47) in Eqs. (41) and (40) and then in Eqs. (35), (36), (38), and (39), we get

$$\pi^{\mu\nu}=2N_FN_c\left\{\frac{1}{2}\big(\Delta^\mu_\sigma\Delta^\nu_\rho+\Delta^\mu_\rho\Delta^\nu_\sigma\big)-\frac{1}{3}\Delta^{\mu\nu}_{\sigma\rho}\right\}\int\frac{d^3\boldsymbol{p}}{(2\pi)^3}\left(\frac{p^\sigma p^\rho}{E}\right)\beta\left(\frac{p^\alpha p^\beta}{E}\right)\big\{\tau_Qf^0_Q\big(1-f^0_Q\big)+\tau_{\bar{Q}}f^0_{\bar{Q}}\big(1-f^0_{\bar{Q}}\big)\big\}\mathcal{U}^\eta_{\alpha\beta}, \tag{48}$$

$$\Pi=2N_FN_c\int\frac{d^3\boldsymbol{p}}{(2\pi)^3}\frac{\beta}{9E^2}\left[\boldsymbol{p}^2-3c_s^2\left(E^2-T^2\frac{dM^2_Q}{dT^2}\right)\right]^2\big\{\tau_Qf^0_Q\big(1-f^0_Q\big)+\tau_{\bar{Q}}f^0_{\bar{Q}}\big(1-f^0_{\bar{Q}}\big)\big\}(\partial_\rho u^\rho), \tag{49}$$

$$q^\mu=2N_FN_c\int\frac{d^3\boldsymbol{p}}{(2\pi)^3}\left(\frac{p^\mu}{E}\right)\beta^2\left(\frac{p^\nu}{E}\right)\big\{\tau_Q(E-h)^2f^0_Q\big(1-f^0_Q\big)+\tau_{\bar{Q}}(E+h)^2f^0_{\bar{Q}}\big(1-f^0_{\bar{Q}}\big)\big\}\mathcal{U}^\kappa_\nu, \tag{50}$$

and

$$J^\mu=2N_c\sum_{Q=u,d}\int\frac{d^3\boldsymbol{p}}{(2\pi)^3}\left(\frac{p^\mu}{E}\right)\beta\left(\frac{p^\nu}{E}\right)\big\{e_Q^2\tau_Qf^0_Q\big(1-f^0_Q\big)+e_{\bar{Q}}^2\tau_{\bar{Q}}f^0_{\bar{Q}}\big(1-f^0_{\bar{Q}}\big)\big\}E_\nu\,. \tag{51}$$

Now, if we compare Eqs. (48)–(51) with Eqs. (29)–(32), then we can identify the final expressions of transport coefficients as

$$\eta = \frac{2N_F N_c \beta}{15}\int \frac{d^3\boldsymbol{p}}{(2\pi)^3}\left(\frac{\boldsymbol{p}^2}{E}\right)^2 \{\tau_Q f_Q(1-f_Q)+\tau_{\bar{Q}} f_{\bar{Q}}(1-f_{\bar{Q}})\}, \tag{52}$$

$$\zeta = \frac{2N_F N_c \beta}{9}\int \frac{d^3\boldsymbol{p}}{(2\pi)^3}\frac{1}{E^2}\left[\boldsymbol{p}^2 - 3c_s^2\left(E^2 - M_Q T\frac{dM_Q}{dT}\right)\right]^2 \{\tau_Q f_Q(1-f_Q)+\tau_{\bar{Q}} f_{\bar{Q}}(1-f_{\bar{Q}})\}, \tag{53}$$

$$\kappa = \frac{2N_F N_c \beta^2}{3}\int \frac{d^3\boldsymbol{p}}{(2\pi)^3}\left(\frac{\boldsymbol{p}}{E}\right)^2 \{\tau_Q (E-h)^2 f_Q(1-f_Q)+\tau_{\bar{Q}} (E+h)^2 f_{\bar{Q}}(1-f_{\bar{Q}})\}, \tag{54}$$

and

$$\sigma = \left(\frac{2N_c\beta}{3}\right)\left(\frac{5e^2}{9}\right)\int \frac{d^3\boldsymbol{p}}{(2\pi)^3}\left(\frac{\boldsymbol{p}}{E}\right)^2 \{\tau_Q f_Q(1-f_Q)+\tau_{\bar{Q}} f_{\bar{Q}}(1-f_{\bar{Q}})\}. \tag{55}$$

Here, the speed of sound is $c_s^2 = \frac{s}{T(\frac{ds}{dT})_V}$. To simplify the notation, we have put $f_{Q,\bar{Q}}$ in the last expressions instead of $f^0_{Q,\bar{Q}}$. We will consider $f_{Q,\bar{Q}}$ as an equilibrium distribution function for the last expressions and all other sections and subsections. The FD distribution will be taken as the equilibrium distribution for the NJL model, whereas the modified distribution, given in Eq. (9), will be considered as the equilibrium distribution for the PNJL or EPNJL models. This replacement calculation for transport coefficients can be found in Ref. [30]. Here also we have addressed the same in Appendix 2.

A. Causal aspects

Now, the above diffusion relations, Eqs. (29), (31), and (32) do not carry any time information, they are instantaneous relations and, therefore, violate the causality. Among the huge number of references on it, readers can follow Refs. [61,64–69] for causal aspects in viscosity, thermal conductivity, and electrical conductivity. Here, we will go through causal aspects in shear viscosity estimation only.

To understand the acausality problem of the Navier-Stokes equation, if we can consider a very small perturbation in energy density $\epsilon \to \epsilon + \delta\epsilon$ and fluid velocity $u^\mu \to u^\mu + \delta u^\mu$, then we will get a dispersion relation of diffusion Eq. (29) as [64]

$$\omega = \frac{\eta}{\epsilon + p}k^2, \tag{56}$$

where k is the wave vector. Hence, we can get diffusion speed,

$$v_T(k) = \frac{d\omega}{dk} = 2\frac{\eta}{\epsilon + P}k, \tag{57}$$

which means diffusion speed can be infinite (by crossing the speed of light) as k tends to infinity. The Navier-Stokes equation (29) is actually derived from first-order thermodynamics. But if we consider entropy density up to second order, then we can obtain causal hydrodynamics equations ([64,65,70]),

$$\pi^{\mu\nu} = \eta\big(D^\mu u^\nu + D^\nu u^\mu - \tfrac{2}{3}\Delta^{\mu\nu}D_\alpha u^\alpha + \pi^{\mu\nu}TD(\beta_2/T) - 2\beta_2 D\pi^{\mu\nu} - \beta_2\pi^{\mu\nu}\partial_\alpha u^\alpha\big), \tag{58}$$

which is the causal replacement of Eq. (29). Realizing the new coefficient β_2 as $\beta_2 = \frac{\tau_\pi}{2\eta}$, where τ_π is defined as the shear relaxation time, we can get the dispersion relation for Eq. (58) as [64]

$$\omega - i\frac{\eta}{\epsilon + p}\frac{k^2}{1 + i\omega\tau_\pi} = 0. \tag{59}$$

Then the diffusion speed at very large k becomes

$$v_T^{\max} \equiv \lim_{k\to\infty}\sqrt{\frac{\eta}{(\epsilon + P)\tau_\pi}}. \tag{60}$$

Here, the subscript T stands for transverse velocity. The diffusion speed will not be greater than the speed of light if

$$\tau_\pi \geqslant \frac{\eta}{\epsilon + P}, \tag{61}$$

which is observed for all known fluids. One can recover the instantaneous Eq. (29) by using $\tau_\pi = 0$. This fact will be well explored in Sec. IV B with different extensions of the NJL model.

IV. RESULTS

A. $\mu = 0$ case

In Sec. II, we have discussed the formalism of different extension components of NJL models such as: (a) vector interaction (Sec. II A), (b) PNJL (Sec. II B), and (c) EPNJL (Sec. II C). The present article is intended to investigate the comparative role of these different extensions of NJL models on transport coefficients of quark matter where we will discuss the results for the $\mu = 0$ case in this subsection. Before that, let us see the thermodynamical quantity, such as entropy density, which will be required to measure the fluid property of quark matter. The governing expression is Eq. (18). Figure 3 shows the T dependence of (normalized) entropy density where a straight horizontal line (black solid line) denotes its massless value ($s \approx 9.2T^3$), commonly known as the Stefan-Boltzmann (SB) limit. Now, the interaction reduces that value as shown by the dotted red, dashed-dot blue, and dashed green lines in Fig. 3, which are obtained from the NJL, EPNJL, and PNJL models, respectively. Through these different extended effective QCD models, interaction is mainly mapped through T-dependent masses $M(T)$, shown earlier in Fig. 2. Since the thermodynamical phase-space part of s is mainly controlled by $M(T)$, one can mark a similar kind of transition pattern

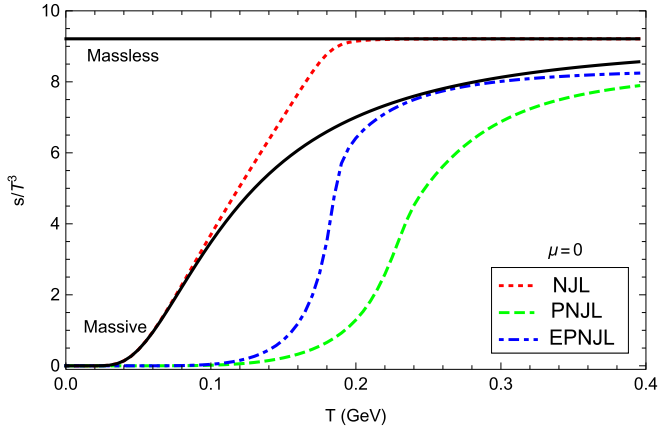

FIG. 3. Normalized entropy density s/T^3 vs temperature T for massive quarks based on the NJL (dotted line), the EPNJL (dashed-dot line), and the PNJL (dashed line) models. As limiting cases we have also shown plots for massless (horizontal solid black line) and massive (black solid line) quarks using the standard FD distribution function. For massive quarks we used confinement mass, which is calculated to be 326 MeV.

between $M(T)$ and $s(T)$. High-T entropy density s of the PNJL and EPNJL models is suppressed from the SB limits because the FD distributions of the NJL model are replaced by their respective modified Polyakov loop distribution. We have also added a curve for constant confinement mass $M = 0.326$ GeV, shown by the black solid line, drawn using the standard Fermi-Dirac distribution function. It is included to demonstrate that the effective models recover this limiting value at low temperatures. Thus, all the models (NJL, PNJL, and EPNJL) basically reproduce or approach the massive and massless limits at $T \to 0$ and $T \to \infty$, respectively.

Next, we come to the transport coefficients estimations from Eqs. (52), (54), (55), and (53). If we note the expressions of transport coefficients in Eqs. (52), (55), (54), and (53) then we can identify two parts, carrying the temperature- (T) and chemical potential- (μ) dependent information. One is the relaxation time of the medium constituent, and another is the thermodynamical part, influenced by its Fermi-Dirac-modified distribution function as well as the $(T, \mu$-) dependent mass. At $\mu = 0$, shear viscosity η, bulk viscosity ζ, and electrical conductivity σ are relevant transport coefficients as thermal conductivity κ is diverged and not well defined at $\mu = 0$. Hence, to zoom in the thermodynamical phase-space part of η, σ, and ζ, we have plotted $\eta/(\tau T^4)$, $\sigma/(\tau T^2)$, and $\zeta/(\tau T^4)$ vs T in Figs. 4(a)–4(c) respectively. Interestingly, we can find a similar kind of pattern in $\eta/(\tau T^4), \sigma/(\tau T^2)$ as we have found for s/T^3. It is because all are basically mapping approximately similar kinds of (normalized) thermodynamical phase-space components. Therefore, according to their rapid changing point on the temperature axis, different extended models follow the same ranking. NJL melts first at low T, then EPNJL and then PNJL at relatively high T. Bulk viscosity in Fig. 4(c) shows peaks near the transition temperatures of the respective models as expected [19]. There will be two sources for which the bulk viscosity contribution becomes maximum near the transition temperature. The first

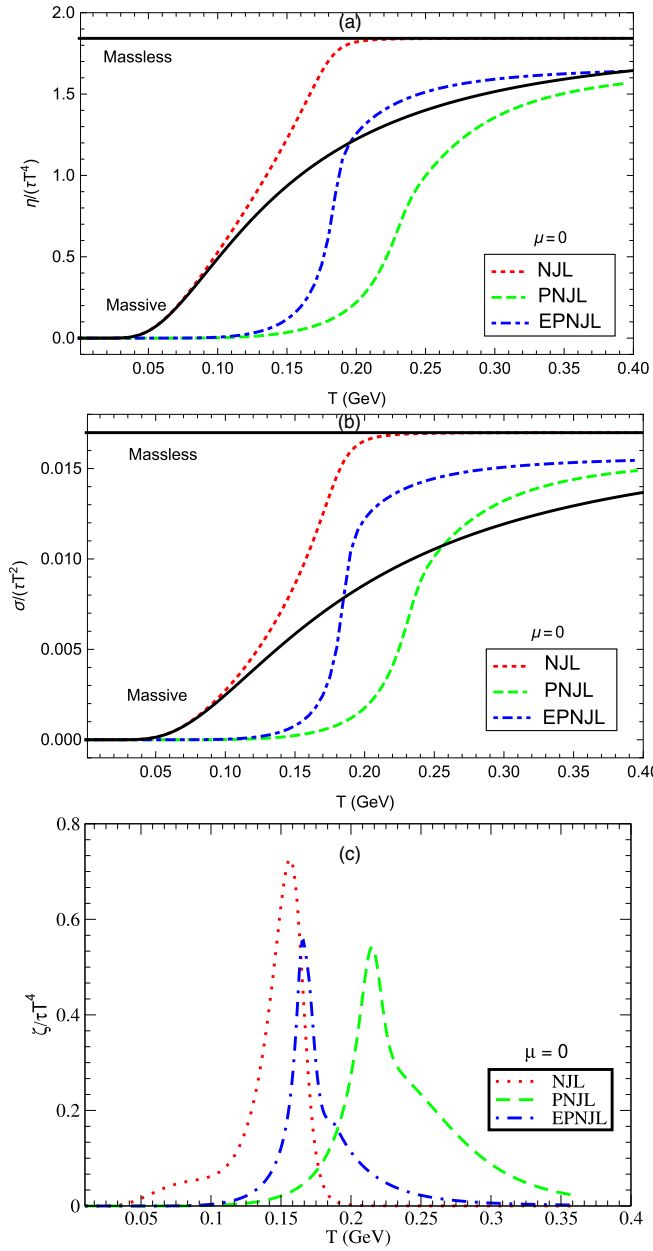

FIG. 4. Normalized (a) shear viscosity $\eta/(\tau T^4)$, (b) electrical conductivity $\sigma/(\tau T^2)$, and (c) bulk viscosity $\zeta/(\tau T^4)$ vs temperature T for massive quarks based on the NJL (dotted line), the EPNJL (dash-dotted line), and the PNJL (dashed line) models. As limiting cases we have also shown plots for massless (horizontal solid black line) and massive (black solid line) quarks using the standard FD distribution function. For massive quarks we used confinement mass, which is calculated to be 326 MeV.

and dominant source is the interaction measure of thermodynamics $\epsilon - 3P$, which is vanishing in the massless medium- or high-temperature QCD media but becomes nonzero in the intermediate- and low-temperature regions. The LQCD as well as the effective QCD model calculations, such as NJL exhibit the maximum interaction measure near the transition temperature. Being proportional with interaction measure $[\zeta \propto (\epsilon - 3P)]$, bulk viscosity displays a similar kind of

TABLE I. Locations of temperatures (MeV) where different temperature-dependent quantities—quark condensate Σ, Polyakov loop Φ, s/T^3, $\eta/(\tau T^4)$, $\sigma/(\tau T^2)$ show their change and transition (for the $\mu = 0$ case).

Models	Σ	Φ	s/T^3	$\eta/(\tau T^4)$	$\sigma/(\tau T^2)$
NJL	177		Two-peak	165	172
PNJL	233	228	230	230	232
EPNJL	185	183	184	183	185

peak structure near the transition temperature. This interaction measure can alternatively be understood as $(\frac{1}{3} - c_s^2)$, which basically interprets the deviation of the speed of the sound square from its massless value of 1/3. This $\zeta \propto (\frac{1}{3} - c_s^2) \propto (\epsilon - 3P)$ relation is, thus, the main source for exhibiting the peak pattern of bulk viscosity, which alternatively reveals the conformal breaking structure of the QCD medium [19]. Another source is the quantity $\frac{dM}{dT}$, which shows the peak structure near chiral transition temperature T_Σ. Sitting in the expression of bulk viscosity, $\frac{dM}{dT}$ and $(\frac{1}{3} - c_s^2)$ become two sources to amplify the peak structure.

At the end of Sec. II C, we have discussed quark condensate Σ[2] and Polyakov loop Φ, which change with T to map the chiral and confinement-deconfinement phase transitions, respectively. The order parameter (Σ) can be estimated from the NJL model, whereas the PNJL and EPNJL can describe both order parameters (Σ, Φ). The transition temperatures T_Σ and T_Φ are basically the inflection points, which are calculated by taking the derivative of the corresponding order parameter with respect to T and then finding the extremum for that. The quantities s/T^3, $\eta/(\tau T^4)$, and $\sigma/(\tau T^2)$ are quite interesting as they contain the collective effect of both order parameters. Table I documents the values of these temperatures for order parameters—quark condensate Σ, Polyakov loop Φ, and as well as for the quantities s/T^3, $\eta/(\tau T^4)$, and $\sigma/(\tau T^2)$. The temperatures for the transport coefficients and the entropy density have been estimated in the same fashion as it is performed for the order parameters. From the expressions of s/T^3, $\eta/(\tau T^4)$, and $\sigma/(\tau T^2)$, written above, one notes that $\Sigma(T)$ enters through $M(T)$, whereas $\Phi(T)$ enters through both $M(T)$ and thermal distribution functions. Although two order parameters enter in the expressions of s/T^3, $\eta/(\tau T^4)$, and $\sigma/(\tau T^2)$ in the same ways, but their momentum-dependent integrands are different and, therefore, they are not showing the same temperatures as evident from Table I. The differences are more evident for the NJL model; as one introduces the background gauge field in the PNJL or EPNJL model the differences almost vanish and the temperatures calculated from these quantities are almost similar to those calculated from the order parameters. Only s/T^3 in the NJL model exhibits the two-peak structure instead of one peak, which is a model-parameter-dependent fact. So, ignoring this fact we can roughly conclude that the transition

[2]Not to be confused with electrical conductivity.

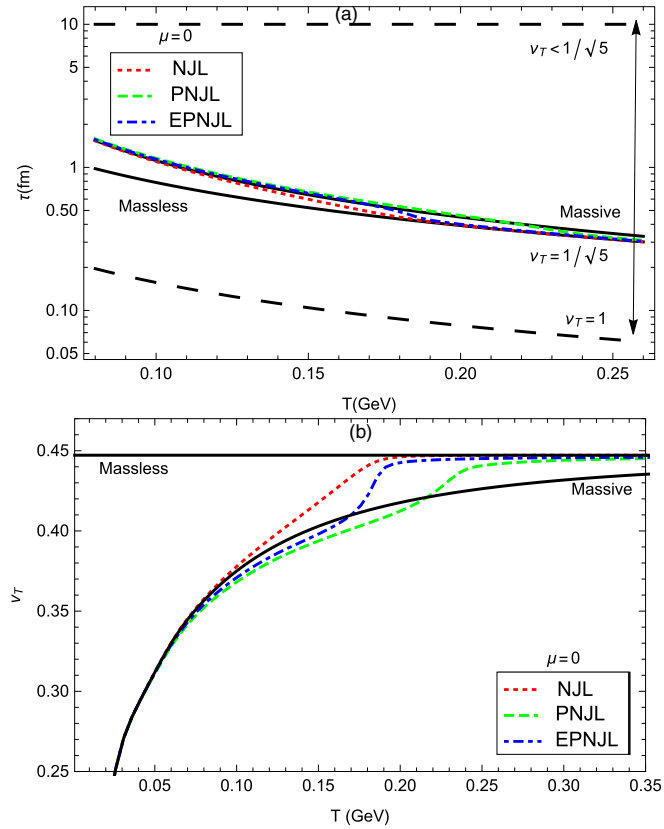

FIG. 5. (a) Temperature dependence of the relaxation time in the NJL, PNJL, and EPNJL models for which we get $\eta/s = 1/4\pi$. For comparison we have also given plots for massless and massive (with confinement mass, 326 MeV) quarks using standard FD statistics. (b) Corresponding maximum values of diffusion speed v_T.

points of s/T^3, $\eta/(\tau T^4)$, and $\sigma/(\tau T^2)$ are close to average values of T_Σ and T_Φ for the PNJL and EPNJL models.

B. Perfect fluid and causal aspects

We have normalized information of τ during plotting shear viscosity in Fig. 4, but it can also be a temperature-dependent quantity if one attempts to calculate it microscopically, and $\tau(T)$ can modify the T-dependent profile of shear viscosity as well as other transport coefficients. From the experimental side, η/s of the quark matter created at RHIC is found to be very close to its lower bound $\frac{1}{4\pi}$, based on viscous hydrodynamic model analysis of elliptic flow [13]. We may get a rough idea about the values of τ for which our estimated η/s will be close to the lower bound. This restriction also gives us a temperature-dependent τ instead of its constant value. For a massless spin-1/2 particle with zero chemical potential, $\tau = 5/4\pi T$ gives us $\eta/s = 1/4\pi$. This is shown as the black line in Fig. 5. Imposing the same restriction of $\eta/s = 1/4\pi$ in the NJL, PNJL, and EPNJL model calculations, we get required relaxation time $\tau(T)$, displayed by dotted, dashed, and dashed-dot lines in Fig. 5. Let us analyze these curves. We know that (approximately) the massless quark can only be expected at very high temperatures, but as we decrease the temperature, the nonzero quark condensate will form for

which constituent quark mass also grows up. Mapping this fact via the gap equation in the NJL model, the thermodynamical part of η becomes suppressed in the low-temperature domain with respect to the massless case. This lower value of the thermodynamical part can be compensated by little higher values of τ for getting the same values of η/s $(= 1/4\pi)$ as obtained in the massless case. Therefore, the red dotted line (τ of the NJL model) is quite larger than the black solid line (τ of the massless case) in the low-temperature domain. Above the transition temperature, both curves are merged as the condensate melts down completely. When we transit to the PNJL model, the confinement picture has been taken into consideration (statistically) via the modified thermal distribution function, which has lower statistical weight than the FD distribution. So, with respect to the NJL case, PNJL has lower strength for the thermodynamical part of η, so for getting KSS[3] limits of η/s, it needs little larger values of τ, shown by the green dashed line in Fig. 5. The EPNJL curve sits in between the NJL and the PNJL curves as expected from their $M(T)$ pattern in Fig. 2.

In Sec. IV B, we have discussed the causal aspects of dissipation phenomena. Dissipation current and forces are linked instantaneously by Eqs. (29), (31), and (32), which means they are communicated via infinite diffusion velocity ($v_T \to \infty$) and, hence, causally disconnected. Through Eq. (58), the causal connection between the shear-channel force and the current can be established by introducing finite shear relaxation time τ_π. The relaxation time τ, discussed earlier, can be called the collisional relaxation time to distinguish it from shear relaxation time τ_π. To zoom in their differences, one can think of τ as a microscopic timescale, which is originated from microscopic collision, whereas τ_π can be considered as a macroscopic timescale, required to satisfy causality. In practice, we take $\tau_\pi \approx \tau$ but actually they are different timescales, which is pointed out in Ref. [61]. A rigorous relation in RTA [66] can connect them by relation,

$$\begin{aligned}\tau_\pi &= \tau\left(\frac{u^\mu k_\mu}{T}\right)^\lambda \\ &= \tau\left(\frac{E}{T}\right)^\lambda \text{(in the fluid rest frame)}\,, \end{aligned} \tag{62}$$

where λ is the unknown parameter. So the inequality, given in Eq. (61), will get a rigorous form

$$\begin{aligned} \tau_\pi &> \frac{\eta}{(\epsilon + P)}, \\ \tau\left(\frac{E}{T}\right)^\lambda &> \frac{\beta_\pi \tau}{(\epsilon + P)}, \\ \Rightarrow \quad v_T^{\max} &= \sqrt{\frac{\beta_\pi}{(\epsilon + P)}\left(\frac{T}{E}\right)^\lambda} < 1, \end{aligned} \tag{63}$$

where $\eta = \beta_\pi \tau$ is assumed. In general, we consider $\lambda = 0$, which means $\tau_\pi = \tau$, i.e., the inequality becomes

$$v_T^{\max} = \sqrt{\frac{\beta_\pi}{(\epsilon + P)}} < 1. \tag{64}$$

The maximum value of diffusion speed, from Eq. (60), can be written for the massless case as

$$v_T^{\max} \equiv \sqrt{\frac{\tau}{5\tau_\pi}}, \tag{65}$$

since $\eta = \tau(\epsilon + P)/5$ for the massless fermionic-bosonic medium. Now, one can easily recognize that $\tau_\pi \to 0$ in Eq. (60) or (65) give us $v_T^{\max} \to \infty$. Hence, to mention relativistic inequality $v_T^{\max} \leqslant 1$, the massless matter should follow the inequality:

$$\tau_\pi \geqslant \frac{\tau}{5}. \tag{66}$$

This lower limit of τ_π $(= \tau/5)$ is drawn by the long dashed line in Fig. 5(a). So, in principle, τ_π can be lower or greater than τ, but we can bound it within the inequality: $\frac{\tau}{5} \leqslant \tau_\pi \leqslant$ 10 fm where the upper limit has been fixed from the phenomenological side by assuming the 10-fm lifetime of the medium (shown by the straight horizontal long dashed line). For the $\tau_\pi \approx \tau$ approximation, the $v_T^{\max} = 1/\sqrt{5}$ massless case and $v_T^{\max}(T)$ for the NJL, PNJL, and EPNJL models are drawn in Fig. 5(b) where all curves follow $v_T^{\max} \leqslant 1/\sqrt{5}$ since we assume $\tau_\pi \approx \tau$. However, we should accept that the general form of $v_T^{\max}$ (at $\mu = 0$),

$$v_T^{\max} = \sqrt{\left(\frac{T}{E}\right)^\lambda \left[\frac{\frac{\beta}{15}\int \frac{d^3\boldsymbol{p}}{(2\pi)^3}\left(\frac{\boldsymbol{p}^2}{E}\right)^2 f_Q(1 - f_Q)}{\int \frac{d^3\boldsymbol{p}}{(2\pi)^3}\left(\frac{\boldsymbol{p}^2}{3E} + E\right) f_Q}\right]}, \tag{67}$$

whose massless limit should be

$$\lim_{m\to 0} = \sqrt{\left(\frac{1}{3}\right)^\lambda \left[\frac{1}{5}\right]}, \tag{68}$$

where roughly the average energy can be considered as $E \approx 3T$. Here, we have generated our numerical values for $\lambda = 0$, i.e., for $\tau_\pi = \tau$ instead of going for any general form. At high T, all are merged to a massless limit as expected, and at low T, the values of $v_T^{\max}(T)$ are quite lower. It means that at the low-T domain, τ_π is quite larger, i.e., quite a safer zone for causal aspects. The inequality $\frac{\tau}{5} \leqslant \tau_\pi \leqslant 10$ fm is shown by the arrow in Fig. 5(a) where the corresponding approximated values of $v_T^{\max}$ are displayed in different zones. Here also, we have put massless ($M = 0$) and confinement mass ($M = 0.300$-GeV) curves (two solid black lines) for $\tau_\pi = \tau$ in Figs. 5(a) and 5(b).

C. Finite μ results

Now, let us move to finite μ results, where we can explore the estimation of thermal conductivity κ, which cannot be studied in the $\mu = 0$ picture. However, thermal diffusion coefficients can be estimated at $\mu = 0$ (see Ref. [61]). We also explore the effect of vector interaction, the incorporation of which becomes almost indispensable at nonzero μ.

[3]KSS (named after the scientists who discovered it, Kovtun-Son-Starinets) is a lower bound on the fluidity of the medium which is the ratio of shear viscosity to entropy density and is found to be equals to $1/4\pi$.

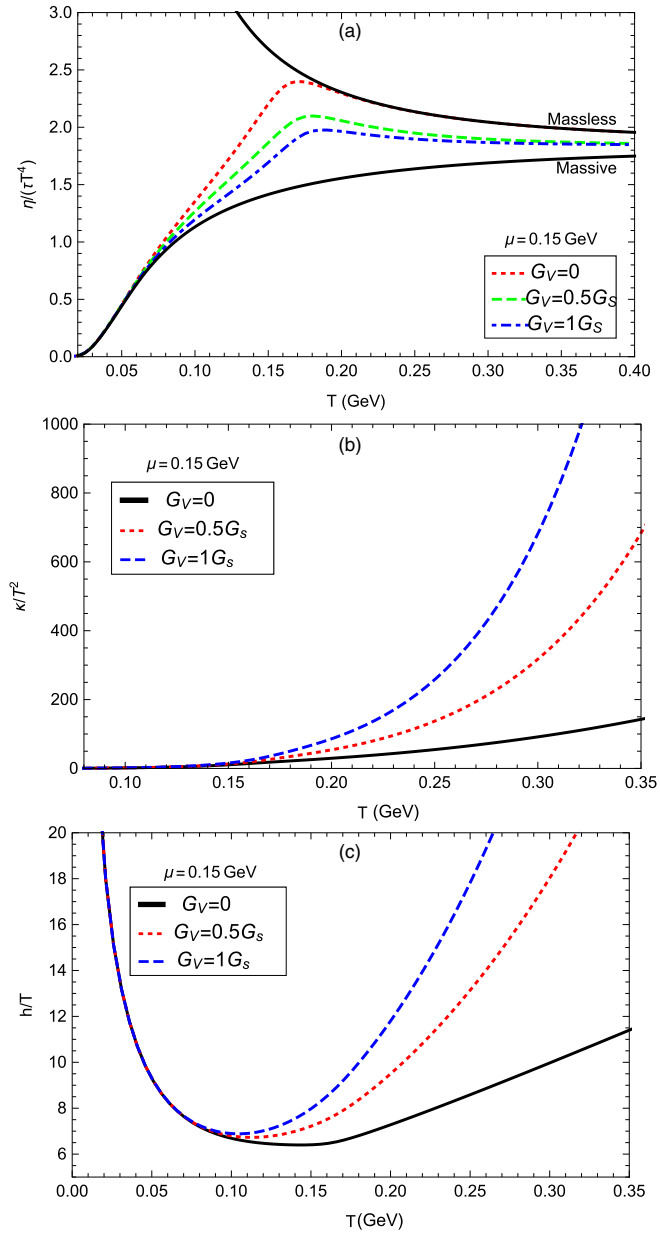

FIG. 6. Finite density plots at different values of G_V for (a) normalized shear viscosity, (b) thermal conductivity, and (c) heat function as a function of T in the NJL model.

In Fig. 6(a), we have plotted $\eta/(\tau T^4)$ against the T axis for $\mu = 0.150$ GeV. For the massless case, instead of a horizontal line as obtained in Fig. 4(a), we are getting a decreasing function of temperature, shown by the black solid line in Fig. 6(a). To understand the blowing trend in the low-temperature range, let us see an analytic form of T dependence for finite μ by taking some rough assumption, described below.

For $\mu = 0$, the massless results of Eq. (52) are

$$\frac{\eta}{\tau T^4} = \left(\frac{7}{8}\right)\left(\frac{\pi^4}{90}\right)\left(\frac{4(4N_F N_c)}{5\pi^2}\right) \approx 1.84, \tag{69}$$

which can be approximated as

$$\frac{\eta}{\tau T^4} = \left(\frac{4(4N_F N_c)}{5\pi^2}\right) \approx 1.94\,, \tag{70}$$

if we take the Maxwell-Boltzmann distribution in place of the Fermi-Dirac distribution of the quark. Now, for $\mu \neq 0$, Eq. (70) can get a simplified form

$$\begin{aligned}\eta &\approx 2N_f N_c \frac{\beta}{15}\int \frac{d^3\boldsymbol{p}}{(2\pi)^3}\tau\left(\frac{\boldsymbol{p}^2}{E}\right)^2 [e^{-\beta(E-\mu)}+e^{-\beta(E+\mu)}] \\ &= 2N_f N_c \frac{\beta}{15}\int \frac{d^3\boldsymbol{p}}{(2\pi)^3}\tau \boldsymbol{p}^2 e^{-\beta E}[e^{\beta\mu}+e^{-\beta\mu}] \\ &= 2N_F N_c \frac{4\tau T^4}{5\pi^2}[e^{\beta\mu}+e^{-\beta\mu}] \\ \Rightarrow \frac{\eta}{\tau T^4} &= 1.94\cosh(\mu/T),\end{aligned} \tag{71}$$

which can explain the blowing up nature of the black solid line in Fig. 6(a) when we decrease the temperature. Now if we revisit again Fig. 4(a), then we see that transition from $m = 0$ to nonzero $M(T)$ provides a large suppression at the low-T domain, which is realized as the effect of the nonperturbative QCD interaction. Hence, in the $\mu \neq 0$ picture, the transition of $m = 0 \to M(T)$ makes the blowing up (black solid) curve be transformed to the (red dotted) suppressed curve. Due to this turning, we will get a peaklike behavior around $T = 160$ MeV. Now we know that with the increase in μ, the transition temperature (T_Σ) decreases. Similarly, transition points for transport coefficients, such as $\eta/(\tau T^4)$, $\sigma/(\tau T^2)$ as well as thermodynamical quantities, are also noted to be shifted towards lower temperatures as μ increases.

Now let us come to the vector interaction picture of the NJL model. As we introduce the vector interaction the transition temperature gets modified for a given chemical potential—it starts increasing with the strength of G_V, which basically couples to the chemical potential through the relation $\tilde{\mu} = \mu - G_V n$, $\tilde{\mu}$ being the effective chemical potential. It means that if we increase the value of G_V the value of the effective chemical potential decreases, thus, the transition temperature increases. A similar transition in the peaklike appearance of $\eta/(\tau T^4)$ is observed, and it shifts towards higher T as G_V is increased. Apart from the transition points, Fig. 6(a) also shows a decreasing profile for increasing G_V. The reason for the reduction of the transport coefficient with vector interaction can be realized as follows. We have already seen in Sec. II A and in Fig. 1, the constituent mass M is slightly enhanced with G_V near the transition temperature. On the other hand, the effective chemical potential $\tilde{\mu}$ decreases with G_V. These increasing M's and decreasing $\tilde{\mu}$'s make the thermodynamical phase-space part of η reduce.

Similar to shear viscosity, the electrical conductivity follows the same pattern (not shown), but totally different variation can be found for thermal conductivity as shown in Fig. 6(b). For thermal conductivity, heat function h, or more precisely enthalpy density per net baryon-quark density plays an important role. Its temperature dependence is shown in Fig. 6(c) where we see that h increases with G_V at high temperatures, which dominantly appear in κ. Now, the reason for

increasing h with G_V can be understood as follows. Increasing G_V makes $\tilde{\mu}$ decrease, and so, ρ decreases. Hence, $h \propto 1/\rho$ increases.

V. SUMMARY

The present article has attempted to explore the effect of different extended components of mean-field models on transport coefficient calculations and made a comparison among them. First we start with the NJL model which can map chiral phase transition of the QCD medium. Here, the quark condensate melts down near the chiral transition temperature, around which normalized transport coefficients and the thermodynamical quantity, such as entropy density, also face maximum changes. Whereas, bulk viscosity is showing peak structure near the transition temperaturelike interaction measure of QCD thermodynamics, observed in LQCD and effective QCD model calculations. Hence, they may be roughly considered as alternative quantities for mapping chiral phase transition. Then to mimic QCD further closely we incorporate the deconfinement dynamics along with the chiral one by taking into account the background gauge field through the PNJL model. Along with the chiral transition temperature, one can separately identify the deconfinement temperature where the Polyakov loop faces a rapid change. The transport coefficients along with thermodynamical quantities will exhibit quite an interesting profile as they contain both chiral and deconfinement dynamics. Hence, they show their signals, such as maximum change (shear viscosity and electrical conductivity) or maximum value (bulk viscosity) around an intermediate temperature between chiral and deconfinement transition temperatures. After the PNJL model, we have considered the EPNJL model, which incorporates a strong entanglement between the chiral and the deconfinement dynamics to enforce the coincidence of chiral and deconfinement transition temperatures within the range provided by the LQCD. Due to this merging of two transition temperatures, we note that order parameters (the quark condensate and the Polyakov loop), normalized-thermodynamical quantities, such as entropy density and normalized-transport coefficients, such as shear viscosity and electrical conductivity, are showing their maximum changes or transitions near the same temperature. Bulk viscosity will show a peak at that temperature. The massless case and the NJL model calculations of transport coefficients are coincided at high temperatures, but the PNJL and EPNJL results still remain suppressed at high temperatures due to the transformation of Fermi-Dirac to the modified distribution function.

After exploring the thermodynamical phase-space components of transport coefficients, we have tried to estimate the relaxation time of quarks from the phenomenological understanding, which expects that the shear viscosity to the entropy density ratio will be very close to the KSS bound. Imposing that phenomenological expectation, required relaxation time from the massless case to the NJL, to the EPNJL to the PNJL models become larger at low temperatures, but they merge at high temperatures. Defining a shear relaxation time to satisfy the causal aspect in the fluid, we have shown its possible range for the RHIC-LHC matter. In normal practice, the (macroscopic) shear relaxation time is considered to be equal with the (microscopic) particle relaxation time, but, in reality, the former timescale might be larger or smaller than the latter one. It is causality, which dictates that the shear diffusion speed in the medium should not exceed the speed of light for which we get the lower limit of the shear relaxation time. On the other hand, the medium lifetime might be considered as the upper limit of the shear relaxation time. Since shear diffusion speed from the massless case to model calculations faces large suppression at low temperatures, therefore, we can say that the nonperturbative low-temperature zone of QCD is causally the more safer zone.

At the end, we have studied the finite quark chemical potential zone of quark matter. Similar features of the decreasing transition temperature with the increasing chemical potential is reflected through the appropriate shift of a peaklike appearance of normalized transport coefficients to a lower value of temperature. The role of vector interaction in the NJL model and estimation of thermal conductivity at the finite quark chemical potential are also investigated.

ACKNOWLEDGMENTS

C.A.I. thanks his institute, the Tata Institute of Fundamental Research (India) funded by the Department of Atomic Energy (DAE), Government of India. S.G. and J.D. acknowledge IIT Bhilai, funded by the Ministry of Human Resource Development (MHRD), Government of India. We are thankful to A. Jashwal for useful discussions.

APPENDIX

1. Left-hand side of relative biological effectiveness

Here, we will address the detail calculation on the left-hand side of the relative biological effectiveness as given in Eq. (46) and see how it can be converted to different (thermodynamical) gradient tensors, associated with shear viscosity, bulk viscosity, thermal conductivity, and electrical conductivity. The reader can find the corresponding calculations of shear viscosity, the bulk viscosity parts from Refs. [28,53,55], the thermal conductivity part from Refs. [28,55], and the electrical conductivity part from Refs. [56,57] separately, but here we present them in a combined form. The FD distribution function, given in Eq. (45), depends on macroscopic quantities or fluid-element quantities—temperature T, chemical potential μ, and four-velocity u^μ, which can depend on x in the local equilibrium picture. It also depends on the microscopic quantity or the particle quantity—four-momentum p^μ, which will not have any x dependence. So Eq. (45) can be rewritten in the local equilibrium picture as

$$f^0_{Q,\bar{Q}} = 1 \Big/ \left\{ \exp\left(\frac{p^\nu u_\nu(x) \mp \mu(x)}{T(x)} \right) + 1 \right\}. \tag{A1}$$

Using Eq. (A1) in the first term on the left-hand side of Eq. (46), we get

$$\begin{aligned}\frac{p^\mu}{E}\partial_\mu f^0_{Q,\bar{Q}} &= -\frac{\exp\left(\frac{p^\nu u_\nu(x)\mp\mu(x)}{T(x)}\right)}{\left\{\exp\left(\frac{p^\nu u_\nu(x)\mp\mu(x)}{T(x)}\right)+1\right\}^2}\left[\frac{p^\mu}{E}\partial_\mu\left\{\frac{p^\nu u_\nu(x)\mp\mu(x)}{T(x)}\right\}\right]\\ &= -f^0_{Q,\bar{Q}}\left(1-f^0_{Q,\bar{Q}}\right)\left[\frac{p^\mu p^\nu}{ET(x)}\partial_\mu u_\nu(x)-\frac{p^\mu p^\nu u_\nu}{ET^2(x)}\partial_\mu T(x)\mp\frac{p^\mu}{E}\partial_\mu\left(\frac{\mu(x)}{T(x)}\right)\right],\\ &= -f^0_{Q,\bar{Q}}\left(1-f^0_{Q,\bar{Q}}\right)\left[\frac{p^\mu p^\nu}{ET}\left\{\partial_\mu u_\nu(x)-\frac{u_\nu\partial_\mu T(x)}{T}\right\}+\frac{2}{ET}\frac{dM_Q^2}{dT}u^\mu\partial_\mu T\mp\frac{p^\mu}{E}\partial_\mu\left(\frac{\mu(x)}{T(x)}\right)\right]\end{aligned}\tag{A2}$$

Our goal will be to express Eq. (A2) in terms of thermodynamical tensors $\mathcal{U}^{\mu\nu}_\eta$, $\partial_\rho u^\rho$, and $\mathcal{U}^{\mu\nu}_\kappa$, connected with η, ζ, and κ. Using the identity [53],

$$\frac{\partial_\mu T}{T} = u^\alpha\partial_\alpha u_\mu - c_s^2 u_\mu\partial_\alpha u^\alpha,\tag{A3}$$

with the square of the speed of sound $c_s^2 = (\frac{\partial P}{\partial\epsilon})$, we can get

$$\begin{aligned}\frac{p^\mu}{E}\partial_\mu f^0_{Q,\bar{Q}} = -f^0_{Q,\bar{Q}}\left(1-f^0_{Q,\bar{Q}}\right)\Bigg[&\frac{p^\mu p^\nu}{2ET}\left\{D_\mu u_\nu + D_\nu u_\mu - \frac{2}{3}\Delta_{\mu\nu}\partial_\alpha u^\alpha\right\}\\ &-\frac{1}{3ET}\left\{p^\mu p^\nu\left(\Delta_{\mu\nu}+3c_s^2u_\mu u_\nu\right)-3c_s^2T^2\frac{dM_Q^2}{dT}\right\}(\partial_\rho u^\rho)\mp\frac{p^\mu}{E}\partial_\mu\left(\frac{\mu(x)}{T(x)}\right)\Bigg].\end{aligned}\tag{A4}$$

Using Eqs. (A6) and (46), we get

$$\begin{aligned}&-f^0_{Q,\bar{Q}}\left(1-f^0_{Q,\bar{Q}}\right)\left[\frac{p^\mu p^\nu}{2ET}\mathcal{U}^{\mu\nu}_\eta-\frac{1}{3ET}\left\{p^\mu p^\nu\left(\Delta_{\mu\nu}+3c_s^2u_\mu u_\nu\right)-3c_s^2T^2\frac{dM_Q^2}{dT}\right\}(\partial_\rho u^\rho)\right]\\ &\quad= -\left(\frac{p\cdot u}{ET}\right)\frac{1}{\tau_{Q,\bar{Q}}}\left[A^{(Q,\bar{Q})}_{\mu\nu}\mathcal{U}^{\mu\nu}_\eta + Z^{(Q,\bar{Q})}(\partial_\rho u^\rho)\right]f^0_{Q,\bar{Q}}\left(1-f^0_{Q,\bar{Q}}\right).\end{aligned}\tag{A5}$$

Now, from the above equation comparing the coefficients of $\mathcal{U}^{\mu\nu}_\eta$ and $\partial_\rho u^\rho$ on both sides [53],

$$\Rightarrow A^{(Q,\bar{Q})}_{\mu\nu} = \tau_{Q,\bar{Q}}\frac{p_\mu p_\nu}{2E}\quad(\text{using } p\cdot u = E)\tag{A6}$$

and

$$\begin{aligned}Z^{(Q,\bar{Q})} &= -\frac{\tau_{Q,\bar{Q}}}{3E}\left\{p^\mu p^\nu\left(\Delta_{\mu\nu}+3c_s^2u_\mu u_\nu\right)-3c_s^2T^2\frac{dM_Q^2}{dT}\right\}\\ &= \tau_{Q,\bar{Q}}\frac{1}{3E}\left[\boldsymbol{p}^2-3c_s^2\left(E^2-T^2\frac{dM_Q^2}{dT^2}\right)\right]\quad(\text{in the local rest frame}).\end{aligned}\tag{A7}$$

The solution (Eq. A7) is not unique [53]. One can make a shift $Z^{(Q,\bar{Q})}\to Z'^{(Q,\bar{Q})} = Z^{(Q,\bar{Q})} - a - bE$, which can also be true. The unknown constants a, b are associated with particle number and energy conservation, respectively. Here we calculate bulk viscosity for the zero chemical potential ($\mu = 0$), thus, $a = 0$. Now, if we have a particular solution of Eq. (A7) as $Z^{(Q,\bar{Q})}_{\rm par}$ which satisfies the Landau-Lifshitz condition (the fluid frame is at rest with energy flow) then $Z^{(Q,\bar{Q})} = Z^{(Q,\bar{Q})}_{\rm par} - bE$. With the help of the microscopic definition of thermodynamical quantities, such as entropy density (s), heat capacity c_V, and Eq. (49), we can find the bulk pressure as

$$\Pi = 2N_fN_c\beta\int\frac{d^3\boldsymbol{p}}{(2\pi)^3}\frac{Z^{(Q,\bar{Q})}_{\rm par}}{3E}\left[\boldsymbol{p}^2-3c_s^2\left(E^2-T^2\frac{dM_Q^2}{dT^2}\right)\right]\left\{f^0_Q\left(1-f^0_Q\right)+f^0_{\bar{Q}}\left(1-f^0_{\bar{Q}}\right)\right\}(\partial_\rho u^\rho),\tag{A8}$$

and

$$Z^{(Q,\bar{Q})}_{\rm par} = \tau_{Q,\bar{Q}}\frac{1}{3E}\left[\boldsymbol{p}^2-3c_s^2\left(E^2-T^2\frac{dM_Q^2}{dT^2}\right)\right].\tag{A9}$$

Here, we can express the square of the speed of sound at $\mu = 0$ as $c_s^2 = \frac{s}{c_V} = \frac{s}{T(\frac{ds}{dT})_V}$.

Now, Eq. (A2) also carries $\mathcal{U}^{\mu}_{\kappa}$, related to κ, which can be constructed by combining the last two terms of Eq. (A2),

$$
\begin{aligned}
-\frac{p^{\mu}(p\cdot u)\partial_{\mu}T(x)}{ET^2}\mp\frac{p^{\mu}}{E}\partial_{\mu}\left(\frac{\mu(x)}{T(x)}\right) &= \frac{p^{\mu}}{E}\left\{-\frac{(p\cdot u)\partial_{\mu}T(x)}{T^2}\mp\partial_{\mu}\left(\frac{\mu(x)}{T(x)}\right)\right\}\\
&\equiv \frac{p^{i}}{E}\left\{-\frac{E\,\partial_{i}T(x)}{T^2}\mp\partial_{i}\left(\frac{\mu(x)}{T(x)}\right)\right\}(\text{using } p\cdot u=E \text{ and } p^{\mu}\equiv p^{i})\\
&= \frac{p^{i}}{E}\left\{\frac{E}{h}\mp 1\right\}\partial_{i}\left(\frac{\mu(x)}{T(x)}\right)\left[\text{Eq. (33) with } \partial_{i}P=0 \text{ is } -\frac{\partial_{i}T}{T^2}=\frac{1}{h}\partial_{i}(\mu/T)\right]. \quad \text{(A10)}
\end{aligned}
$$

Using Eq. (A10) in Eq. (A2) and then in Eq. (46), we get

$$
\begin{aligned}
-f^{0}_{Q,\bar{Q}}(1-f^{0}_{Q,\bar{Q}})\frac{p^{i}}{E}\left\{\frac{E}{h}\mp 1\right\}\partial_{i}\left(\frac{\mu(x)}{T(x)}\right)+\cdots &= -\left(\frac{p\cdot u}{ET}\right)\frac{1}{\tau_{Q,\bar{Q}}}\left[B^{i}\frac{T^2}{h}\partial_{i}\left(\frac{\mu(x)}{T(x)}\right)+\cdots\right]f^{0}_{Q,\bar{Q}}(1-f^{0}_{Q,\bar{Q}})\\
\Rightarrow B^{i}_{(Q,\bar{Q})} &= \tau_{Q,\bar{Q}}\frac{p_{i}}{ET}(E\mp h) \quad (\text{using } p\cdot u=E)\\
\Rightarrow B^{\mu}_{(Q,\bar{Q})} &= \tau_{Q,\bar{Q}}\frac{p_{\mu}}{ET}(E\mp h). \quad \text{(A11)}
\end{aligned}
$$

On the other hand, the second term on the left-hand side of Eq. (46) can be simplified through the four-vector to the three-vector and again to the four-vector components (i.e., the $\mu\to i\to\mu$ index) as

$$
\begin{aligned}
e_{Q,\bar{Q}}F^{\mu\nu}\frac{p_{\nu}}{E}\frac{\partial f^{0}_{Q,\bar{Q}}}{\partial p^{\mu}} \equiv e_{Q,\bar{Q}}E^{i}\frac{\partial f^{0}_{Q,\bar{Q}}}{\partial p^{i}} &= -f^{0}_{Q,\bar{Q}}(1-f^{0}_{Q,\bar{Q}})\left[e_{Q,\bar{Q}}E^{i}\frac{\partial}{\partial p^{i}}\left(\frac{E}{T}\right)\right]\\
&= -f^{0}_{Q,\bar{Q}}(1-f^{0}_{Q,\bar{Q}})\left[e_{Q,\bar{Q}}\frac{\vec{E}\cdot\vec{p}}{ET}\right]=-f^{0}_{Q,\bar{Q}}(1-f^{0}_{Q,\bar{Q}})\left[e_{Q,\bar{Q}}\frac{E_{\mu}p^{\mu}}{ET}\right]. \quad \text{(A12)}
\end{aligned}
$$

Since in electromagnetic-field tensor $F^{\mu\nu}$, there are only electric fields (as no external magnetic field is considered in the present paper), so $F^{\mu\nu}\frac{p_{\nu}}{E}=F^{0\mu}+F^{ij}\frac{p_{j}}{E}+\cdots=F^{0\mu}=E^{\mu}$ is used in the above calculations.

Using Eq. (A12) in Eq. (A2) and then in Eq. (46), we get

$$
-f^{0}_{Q,\bar{Q}}(1-f^{0}_{Q,\bar{Q}})\left[e_{Q,\bar{Q}}\frac{E_{\mu}p^{\mu}}{ET}\right]+\cdots=-\left(\frac{p\cdot u}{ET}\right)\frac{1}{\tau_{Q,\bar{Q}}}[C^{(Q,\bar{Q})}_{\mu}E^{\mu}+\cdots]f^{0}_{Q,\bar{Q}}(1-f^{0}_{Q,\bar{Q}})\Rightarrow C^{\mu}=\tau_{Q,\bar{Q}}\frac{e_{Q,\bar{Q}}p^{\mu}}{E}. \quad \text{(A13)}
$$

2. PNJL-EPNJL distribution replacement

The modified distribution function, given in Eq. (9), can be realized as the color average of the FD distribution of the color particle with the imaginary chemical potential [30]. Let us write down the FD distribution with the imaginary chemical potential Q^{i} in the local equilibrium picture as [71]

$$
f^{i}_{Q,\bar{Q}}=1\Big/\left\{\exp\left(\frac{p^{\nu}u_{\nu}(x)\mp\mu(x)\mp Q^{i}}{T(x)}\right)+1\right\}, \quad \text{(A14)}
$$

where $Q^{i}=2\pi T(+q,0,-q)$ with dimensionless condensate variable q. The Polyakov loop variable can be expressed as

$$
\Phi=\frac{1}{3}\sum_{i}e^{i\beta Q_{i}}=\frac{1}{3}\{1+2\cos(2\pi q)\}\,. \quad \text{(A15)}
$$

Let us rename the modified distribution function as f_{Φ} and rewrite as

$$
f^{\Phi}_{Q,\bar{Q}}=\frac{\Phi e^{-\beta(E\mp\mu)}+2\bar{\Phi}e^{-2\beta(E\mp\mu)}+e^{-3\beta(E\mp\mu)}}{1+3\Phi e^{-\beta(E\mp\mu)}+3\bar{\Phi}e^{-2\beta(E\mp\mu)}+e^{-3\beta(E\mp\mu)}}=\frac{N}{D}\ \ (\text{say}). \quad \text{(A16)}
$$

One can easily check the relation between $f^{i}_{Q,\bar{Q}}$ and $f^{\Phi}_{Q,\bar{Q}}$ as

$$
\begin{aligned}
\frac{1}{3}\sum_{i}f^{i}_{Q,\bar{Q}} &= \frac{1}{3}\left[\frac{1}{\exp\{(E\mp\mu\mp i2\pi Tq)/T\}+1}+\frac{1}{\exp\{(E\mp\mu)/T\}+1}+\frac{1}{\exp\{(E\mp\mu\pm i2\pi Tq)/T\}+1}\right]\\
&= \frac{1}{3}\left[\frac{e^{2\beta(E\mp\mu)}\{1+2\cos(2\pi q)\}+2e^{\beta(E\mp\mu)}\{1+2\cos(2\pi q)\}+3}{e^{3\beta(E\mp\mu)}+e^{2\beta(E\mp\mu)}\{1+2\cos(2\pi q)\}+e^{\beta(E\mp\mu)}\{1+2\cos(2\pi q)\}+1}\right]\\
&= \left[\frac{e^{2\beta(E\mp\mu)}\Phi+2e^{\beta(E\mp\mu)}\Phi+1}{e^{3\beta(E\mp\mu)}+3e^{2\beta(E\mp\mu)}\Phi+3e^{\beta(E\mp\mu)}\Phi+1}\right] \quad [\text{using Eq. (A15)}]\\
&= f^{\Phi}_{Q,\bar{Q}}. \quad \text{(A17)}
\end{aligned}
$$

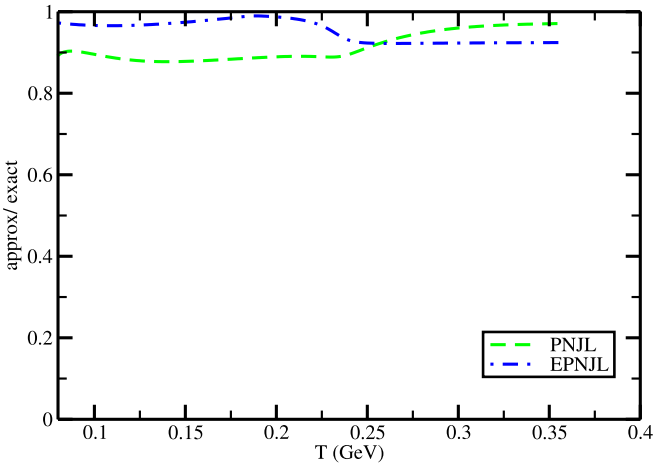

FIG. 7. The ratio between phase-space integration with the approximated (excluding the extra term) and the exact (including the extra term) vs T, whose values close to 1 reflect that one may go with this approximation.

The transport coefficient calculations remain almost the same, and only the terms, associated with the distribution, will have to be recalculated. When we start our journey from the color particle FD distribution $f^i_{Q,\bar{Q}}$ and its color average $\frac{1}{3}\sum f^i_{Q,\bar{Q}}$, then their derivative with respect to E, p_i, and x will have the same anatomy as earlier, i.e.,

$$\frac{1}{3}\sum_i \frac{\partial f^i_{Q,\bar{Q}}}{\partial E} = -\beta\frac{1}{3}\sum_i f^i_{Q,\bar{Q}}(1-f^i_{Q,\bar{Q}}),$$
$$\frac{1}{3}\sum_i \frac{\partial f^i_{Q,\bar{Q}}}{\partial p_i} = -\beta\frac{1}{3}\sum_i \left(\frac{p^i}{E}\right) f^i_{Q,\bar{Q}}(1-f^i_{Q,\bar{Q}}), \tag{A18}$$
$$\frac{1}{3}\sum_i \partial_\mu f^i_{Q,\bar{Q}} = -\frac{1}{3}\sum_i f^i_{Q,\bar{Q}}(1-f^i_{Q,\bar{Q}})\partial_\mu\left\{\frac{p^\nu u_\nu(x)\mp\mu(x)}{T(x)}\right\}.$$

These relations indicate that the anatomy of Eqs. (40), (46), and (A2) remains the same. Only the FD distribution is replaced by a FD distribution of color particles. Now we have to transform the FD distribution of color particles $f^i_{Q,\bar{Q}}$ in Eq. (A19) into the modified distribution function $f^\Phi_{Q,\bar{Q}}$. We can express the terms $f^i_{Q,\bar{Q}}(1-f^i_{Q,\bar{Q}})$ as

$$-\frac{1}{3}\sum_i f^i_{Q,\bar{Q}}(1-f^i_{Q,\bar{Q}}) = \frac{1}{3\beta}\sum_i \frac{\partial f^i_{Q,\bar{Q}}}{\partial E} = \frac{1}{\beta}\frac{\partial f^\Phi_{Q,\bar{Q}}}{\partial E} = \frac{1}{\beta}\frac{\left(D\frac{\partial N}{\partial E} - N\frac{\partial D}{\partial E}\right)}{D^2}. \tag{A19}$$

If we expand the above expression, we can get

$$\begin{aligned}\frac{\left(D\frac{\partial N}{\partial E} - N\frac{\partial D}{\partial E}\right)}{D^2} &= \frac{N}{D}\left(1-\frac{N}{D}\right) + \{2D(\Phi e^{-2\beta(E\mp\mu)} + e^{-3\beta(E\mp\mu)}) - 2N^2\}/D^2 \\ &= f^\Phi_{Q,\bar{Q}}(1-f^\Phi_{Q,\bar{Q}}) + 2e^{-2\beta(E\mp\mu)}[(1+e^{-2\beta(E\mp\mu)})\Phi(1-\Phi) + e^{-\beta(E\mp\mu)}(1-\Phi^2)]/D^2 \\ &\approx f^\Phi_{Q,\bar{Q}}(1-f^\Phi_{Q,\bar{Q}}).\end{aligned} \tag{A20}$$

The extra term in Eq. (A20) might be ignored with respect to the dominating term $f^\Phi_{Q,\bar{Q}}(1-f^\Phi_{Q,\bar{Q}})$. For a numerical check, Fig. 7 has shown the ratio between phase-space integration with approximated (excluding extra term) and exact (including extra term), i.e.,

$$\frac{\chi_{\rm approx}}{\chi_{\rm exact}} = \frac{\int \frac{d^3k}{(2\pi)^3}\left[\beta f^\Phi_0(1-f^\Phi_0)\right]}{\int \frac{d^3k}{(2\pi)^3}\left[-\frac{1}{3}\sum_i \frac{\partial f^i_{Q,\bar{Q}}}{\partial E}\right]}. \tag{A21}$$

We note that the extra term roughly contributes up to 10%. So one may go safely for rough estimation of different transport coefficients with the simplified phase-space factor $[\beta f^\Phi_0(1-f^\Phi_0)]$ instead of its complicated version $[-\frac{1}{3}\sum_i \frac{\partial f^i_{Q,\bar{Q}}}{\partial E}]$ or $\frac{(D\frac{\partial N}{\partial E} - N\frac{\partial D}{\partial E})}{D^2}$. We have shown here susceptibility-type quantity χ, which is basically attached with all transport coefficients, hence, this approximation will be valid during estimation transport coefficients or any other quantities, which are proportionally connected with susceptibility. Owing to this assumption, we have used the replacement identity,

$$-\frac{1}{3}\sum_i f^i_{Q,\bar{Q}}(1-f^i_{Q,\bar{Q}}) \approx -f^\Phi_{Q,\bar{Q}}(1-f^\Phi_{Q,\bar{Q}}), \tag{A22}$$

during the calculation of different transport coefficients in the PNJL and EPNJL models.

[1] I. A. Shovkovy and P. J. Ellis, Thermal conductivity of dense quark matter and cooling of stars, Phys. Rev. C **66**, 015802 (2002).

[2] C. Manuel, A. Dobado, and F. J. Llanes-Estrada, Shear viscosity in a CFL quark star, J. High Energy Phys. 09 (2005) 076.

[3] M. G. Alford, H. Nishimura, and A. Sedrakian, Transport coefficients of two-flavor superconducting quark matter, Phys. Rev. C **90**, 055205 (2014).

[4] S. Sarkar and R. Sharma, The shear viscosity of two-flavor crystalline color superconducting quark matter, Phys. Rev. D **96**, 094025 (2017).

[5] B. Friman, C. Höhne, J. Knoll, S. Leupold, J. Randrup, R. Rapp *et al.*, *The CBM Physics Book: Compressed Baryonic Matter in Laboratory Experiments*, Lecture Notes in Physics (Springer, Berlin/Heidelberg, 2011).

[6] D. Blaschke, J. Aichelin, E. Bratkovskaya, V. Friese, M. Gazdzicki, J. Randrup, O. Rogachevsky, O. Teryaev, and V. Toneev, Topical issue on exploring strongly interacting matter at high densities–nica white paper, Eur. Phys. J. A **52**, 267 (2016).

[7] S. S. Adler *et al.* (PHENIX Collaboration), Elliptic Flow of Identified Hadrons in Au+Au Collisions at s(NN)**(1/2) = 200-GeV, Phys. Rev. Lett. **91**, 182301 (2003).

[8] J. Adams *et al.* (STAR Collaboration), Azimuthal anisotropy in Au+Au collisions at s(NN)**(1/2) = 200-GeV, Phys. Rev. C **72**, 014904 (2005).

[9] K. Aamodt *et al.* (ALICE Collaboration), Higher Harmonic Anisotropic Flow Measurements of Charged Particles in Pb-Pb Collisions at $\sqrt{s_{NN}} = 2.76$ TeV, Phys. Rev. Lett. **107**, 032301 (2011).

[10] S. Chatrchyan *et al.* (CMS Collaboration), Multiplicity and transverse momentum dependence of two- and four-particle correlations in pPb and PbPb collisions, Phys. Lett. B **724**, 213 (2013).

[11] G. Aad *et al.* (ATLAS Collaboration), Measurement of event-plane correlations in $\sqrt{s_{NN}} = 2.76$ TeV lead-lead collisions with the ATLAS detector, Phys. Rev. C **90**, 024905 (2014).

[12] J. Adam *et al.* (ALICE Collaboration), Correlated Event-by-Event Fluctuations of Flow Harmonics in Pb-Pb Collisions at $\sqrt{s_{NN}} = 2.76$ TeV, Phys. Rev. Lett. **117**, 182301 (2016).

[13] M. J. Tannenbaum, Recent results in relativistic heavy ion collisions: from 'a new state of matter' to 'the perfect fluid', Rep. Prog. Phys. **69**, 2005 (2006).

[14] P. Romatschke and U. Romatschke, Viscosity Information from Relativistic Nuclear Collisions: How Perfect is the Fluid Observed at RHIC? Phys. Rev. Lett. **99**, 172301 (2007).

[15] U. Heinz and R. Snellings, Collective flow and viscosity in relativistic heavy-ion collisions, Annu. Rev. Nucl. Part. Sci. **63**, 123 (2013).

[16] P. B. Arnold, G. D. Moore, and L. G. Yaffe, Transport coefficients in high temperature gauge theories. 1. Leading log results, J. High Energy Phys. 11 (2000) 001.

[17] P. B. Arnold, G. D. Moore, and L. G. Yaffe, Transport coefficients in high temperature gauge theories: (II) Beyond leading log, J. High Energy Phys. 05 (2003) 051.

[18] J. Ghiglieri, G. D. Moore, and D. Teaney, QCD shear viscosity at (almost) NLO, J. High Energy Phys. 03 (2018) 179.

[19] S. Ghosh, T. C. Peixoto, V. Roy, F. E. Serna, and G. Krein, Shear and bulk viscosities of quark matter from quark-meson fluctuations in the Nambu–Jona-Lasinio model, Phys. Rev. C **93**, 045205 (2016).

[20] S. Ghosh, F. E. Serna, A. Abhishek, G. Krein, and H. Mishra, Transport responses from rate of decay and scattering processes in the Nambu–Jona-Lasinio model, Phys. Rev. D **99**, 014004 (2019).

[21] S. Ghosh, A. Lahiri, S. Majumder, R. Ray, and S. K. Ghosh, Shear viscosity due to Landau damping from the quark-pion interaction, Phys. Rev. C **88**, 068201 (2013).

[22] R. Lang and W. Weise, Shear viscosity from Kubo formalism: NJL model study, Eur. Phys. J. A **50**, 63 (2014).

[23] R. Lang, N. Kaiser, and W. Weise, Shear viscosities from Kubo formalism in a large-N_c Nambu-Jona-Lasinio model, Eur. Phys. J. A **51**, 127 (2015).

[24] P. Zhuang, J. Hufner, S. P. Klevansky, and L. Neise, Transport properties of a quark plasma and critical scattering at the chiral phase transition, Phys. Rev. D **51**, 3728 (1995).

[25] P. Rehberg, S. P. Klevansky, and J. Hufner, Elastic scattering and transport coefficients for a quark plasma in $SU_f(3)$ at finite temperatures, Nucl. Phys. A **608**, 356 (1996).

[26] C. Sasaki and K. Redlich, Transport coefficients near chiral phase transition, Nucl. Phys. A **832**, 62 (2010).

[27] R. Marty, E. Bratkovskaya, W. Cassing, J. Aichelin, and H. Berrehrah, Transport coefficients from the Nambu–Jona-Lasinio model for $SU(3)_f$, Phys. Rev. C **88**, 045204 (2013).

[28] P. Deb, G. Kadam, and H. Mishra, Estimating transport coefficients in hot and dense quark matter, Phys. Rev. D **94**, 094002 (2016).

[29] A. Abhishek, H. Mishra, and S. Ghosh, Transport coefficients in the Polyakov quark meson coupling model: A relaxation time approximation, Phys. Rev. D **97**, 014005 (2018).

[30] P. Singha, A. Abhishek, G. Kadam, S. Ghosh, and H. Mishra, Calculations of shear, bulk viscosities and electrical conductivity in the Polyakov-quark–meson model, J. Phys. G: Nucl. Part. Phys. **46**, 015201 (2019).

[31] S. K. Ghosh, S. Raha, R. Ray, K. Saha, and S. Upadhaya, Shear viscosity and phase diagram from Polyakov–Nambu–Jona-Lasinio model, Phys. Rev. D **91**, 054005 (2015).

[32] T. Kunihiro, Quark number susceptibility and fluctuations in the vector channel at high temperatures, Phys. Lett. B **271**, 395 (1991).

[33] S. P. Klevansky, The Nambu-Jona-Lasinio model of quantum chromodynamics, Rev. Mod. Phys. **64**, 649 (1992).

[34] T. Hatsuda and T. Kunihiro, QCD phenomenology based on a chiral effective Lagrangian, Phys. Rep. **247**, 221 (1994).

[35] M. Buballa, NJL model analysis of quark matter at large density, Phys. Rep. **407**, 205 (2005).

[36] K. Kashiwa, H. Kouno, T. Sakaguchi, M. Matsuzaki, and M. Yahiro, Chiral phase transition in an extended NJL model with higher-order multi-quark interactions, Phys. Lett. B **647**, 446 (2007).

[37] S. K. Ghosh, T. K. Mukherjee, M. G. Mustafa, and R. Ray, Susceptibilities and speed of sound from PNJL model, Phys. Rev. D **73**, 114007 (2006).

[38] S. Mukherjee, M. G. Mustafa, and R. Ray, Thermodynamics of the PNJL model with nonzero baryon and isospin chemical potentials, Phys. Rev. D **75**, 094015 (2007).

[39] C. Ratti, M. A. Thaler, and W. Weise, Phases of QCD: Lattice thermodynamics and a field theoretical model, Phys. Rev. D **73**, 014019 (2006).

[40] S. K. Ghosh, T. K. Mukherjee, M. G. Mustafa, and R. Ray, PNJL model with a Van der Monde term, Phys. Rev. D **77**, 094024 (2008).

[41] K. Fukushima, Phase diagrams in the three-flavor Nambu-Jona-Lasinio model with the Polyakov loop, Phys. Rev. D **77**, 114028 (2008).
[42] S. K. Ghosh, A. Lahiri, S. Majumder, M. G. Mustafa, S. Raha, and R. Ray, Quark number susceptibility: Revisited with fluctuation-dissipation theorem in mean field theories, Phys. Rev. D **90**, 054030 (2014).
[43] H. Hansen, W. M. Alberico, A. Beraudo, A. Molinari, M. Nardi, and C. Ratti, Mesonic correlation functions at finite temperature and density in the Nambu-Jona-Lasinio model with a Polyakov loop, Phys. Rev. D **75**, 065004 (2007).
[44] C. A. Islam, S. Majumder, N. Haque, and M. G. Mustafa, Vector meson spectral function and dilepton production rate in a hot and dense medium within an effective QCD approach, J. High Energy Phys. 02 (2015) 011.
[45] C. A. Islam, R. Abir, M. G. Mustafa, S. K. Ghosh, and R. Ray, The consequences of SU(3) colorsingletness, Polyakov Loop and $Z(3)$ symmetry on a quark–gluon gas, J. Phys. G: Nucl. Part. Phys. **41**, 025001 (2014).
[46] M. Fukugita and A. Ukawa, Deconfining and Chiral Transitions of Finite Temperature Quantum Chromodynamics in the Presence of Dynamical Quark Loops, Phys. Rev. Lett. **57**, 503 (1986),
[47] Y. Aoki, Z. Fodor, S. D. Katz, and K. K. Szabo, The QCD transition temperature: Results with physical masses in the continuum limit, Phys. Lett. B **643**, 46 (2006).
[48] Y. Sakai, T. Sasaki, H. Kouno, and M. Yahiro, Entanglement between deconfinement transition and chiral symmetry restoration, Phys. Rev. D **82**, 076003 (2010).
[49] J. Sugano, J. Takahashi, M. Ishii, H. Kouno, and M. Yahiro, Determination of the strength of the vector-type four-quark interaction in the entanglement Polyakov-loop extended Nambu–Jona-Lasinio model, Phys. Rev. D **90**, 037901 (2014).
[50] C. A. Islam, S. Majumder, and M. G. Mustafa, Vector meson spectral function and dilepton rate in the presence of strong entanglement effect between the chiral and the Polyakov loop dynamics, Phys. Rev. D **92**, 096002 (2015).
[51] F. Karsch, Lattice QCD at high temperature and density, Lect. Notes Phys. **583**, 209 (2002).
[52] F. Karsch, E. Laermann, and A. Peikert, Quark mass and flavor dependence of the QCD phase transition, Nucl. Phys. B **605**, 579 (2001).
[53] P. Chakraborty and J. I. Kapusta, Quasi-Particle Theory of Shear and Bulk Viscosities of Hadronic Matter, Phys. Rev. C **83**, 014906 (2011).
[54] A. Hosoya and K. Kajantie, Transport coefficients of QCD matter, Nucl. Phys. B **250**, 666 (1985).
[55] S. Gavin, Transport coefficients in ultra-relativistic heavy-ion collisions, Nucl. Phys. A **435**, 826 (1985).
[56] A. Puglisi, S. Plumari, and V. Greco, Electric conductivity from the solution of the relativistic Boltzmann equation, Phys. Rev. D **90**, 114009 (2014).
[57] G. P. Kadam, H. Mishra, and L. Thakur, Electrical and thermal conductivities of hot and dense hadronic matter, Phys. Rev. D **98**, 114001 (2018).
[58] S. Ghosh, A real-time thermal field theoretical analysis of Kubo-type shear viscosity: Numerical understanding with simple examples, Int. J. Mod. Phys. A **29**, 1450054 (2014).
[59] S. Ghosh, Electrical conductivity of hadronic matter from different possible mesonic and baryonic loops, Phys. Rev. D **95**, 036018 (2017).
[60] D. Fernandez-Fraile and A. Gomez Nicola, Transport coefficients and resonances for a meson gas in chiral perturbation theory, Eur. Phys. J. C **62**, 37 (2009).
[61] A. Muronga, Causal theories of dissipative relativistic fluid dynamics for nuclear collisions, Phys. Rev. C **69**, 034903 (2004).
[62] M. Greif, I. Bouras, C. Greiner, and Z. Xu, Electric conductivity of the quark-gluon plasma investigated using a perturbative QCD based parton cascade, Phys. Rev. D **90**, 094014 (2014).
[63] L. J. Anderson and H. R. Witting, A relativistic relaxation-time model for the Boltzmann equation, Physica **74**, 466 (1974)
[64] P. Romatschke, New developments in relativistic viscous hydrodynamics, Int. J. Mod. Phys. E **19**, 1 (2010).
[65] W. Israel and J. M. Stewart, Transient relativistic thermodynamics and kinetic theory, Ann. Phys. (NY) **118**, 341 (1979).
[66] G. S. Denicol, S. Jeon, and C. Gale, Impact of different extended components of mean field models on transport coefficients of quark matter and their causal aspects, Phys. Rev. C **90**, 024912 (2014).
[67] L. P. Csernai, J. I. Kapusta, and L. D. McLerran, Strongly Interacting Low-Viscosity Matter Created in Relativistic Nuclear Collisions, Phys. Rev. Lett. **97**, 152303 (2006).
[68] A. Jaiswal, B. Friman, and K. Redlich, Relativistic second-order dissipative hydrodynamics at finite chemical potential, Phys. Lett. B **751**, 548 (2015)
[69] J. I. Kapusta and C. Plumberg, Causal electric charge diffusion and balance functions in relativistic heavy ion collisions, Phys. Rev. C **97**, 014906 (2018).
[70] William A. Hiscock and L. Lindblom, Stability and causality in dissipative relativistic fluids, Ann. Phys. (NY) **151**, 466 (1983).
[71] Y. Hidaka, S. Lin, R. D. Pisarski, and D. Satow, Dilepton and photon production in the presence of a nontrivial Polyakov loop, J. High Energy Phys. 10 (2015) 005.